Received: 19 November 2019 | Revised: 27 November 2020 | Accepted: 30 November 2020

DOI: 10.1002/we.2605

RESEARCH ARTICLE

WILEY

Harmonic linearisation of aerodynamic loads in a frequency-domain model of a floating wind turbine

Richard C. Lupton[1] | **Robin S. Langley**[2]

[1]Department of Mechanical Engineering, University of Bath, Bath, UK

[2]Department of Engineering, University of Cambridge, Cambridge, UK

Correspondence
Richard C. Lupton, Department of Mechanical Engineering, University of Bath, Claverton Down, Bath BA2 7AY, UK.
Email: R.C.Lupton@bath.ac.uk

Funding information
Engineering and Physical Sciences Research Council, Grant/Award Number: 1089390

Abstract

While detailed aero-servo-hydro-elastic simulation codes for modelling floating wind turbines (FWTs) are available, they achieve high accuracy at the expense of calculation speed. For conceptual design and optimisation, fast solutions are needed, and equivalent linearisation techniques combined with frequency-domain analysis offers to capture the complex behaviour of FWTs in fast, approximate models. The main aim of this paper is to apply a harmonic linearisation approach to model the aerodynamic loading within a complete coupled model of a FWT, quantifying its performance, and where accuracy is unsatisfactory, to give insight into the causes. Two linearised models are derived from a coupled nonlinear aero-hydro-servo-elastic model, using the OC3-Hywind FWT as a test case: the typical tangent linearisation derived by numerical perturbation of the nonlinear model and the harmonic linearisation yielding improved representation of the aerodynamic loads. Comparisons against nonlinear time-domain simulations from Bladed show that it is possible to create a frequency-domain model of a FWT, including a flexible structure, aeroelastic rotor loads and the effect of the control system, with reasonable accuracy. The biggest source of errors is the presence of additional harmonics caused by nonlinear interactions between loads at different frequencies, rather than inaccurate linearisation of the magnitudes of forces. The computational cost of the harmonic linearisation implemented varies, but in most cases is ∼10× slower than the tangent linearisation and ∼100× faster than the time domain solution.

KEYWORDS

aerodynamic loads, equivalent linearisation, floating wind turbine, frequency-domain modelling, harmonic linearisation, nonlinearity

1 | INTRODUCTION

The technical feasibility of floating wind turbines has been demonstrated by prototypes including Hywind,[1] WindFloat[2] and Fukushima-FORWARD.[3] However, compared to other types of wind turbine and other floating offshore structures used in the oil and gas industry, their development is still at an early stage, with the overall aim of reducing the levelised cost of energy (LCOE) produced by the wind turbine to competitive levels.[4] The benefits of achieving this are large, with a potential accessible wind resource estimated as 4,000 GW in Europe,[5] with another 3,000 GW possible in Japan and the United States (for comparison, the current installed offshore wind capacity in Europe is 16 GW[6]). To achieve this,

conceptual design and optimisation have a particularly critical role,[7] but this relies on being able to predict the behaviour of a wide range of different designs, across all conditions, with acceptable accuracy and computational effort.

State-of-the-art simulation codes (e.g., FAST[8] and Bladed[9]) do this through coupled aero-servo-hydro-elastic simulations in the time domain. While these codes are an essential part of the later stages of the design process, they are too slow to systematically explore the potential merit of a wide design space early on in the design process. There is therefore growing interest in approximate models which can run quickly to help to converge on better designs. Pegalajar-Jurado et al.[10] argue that better design tools would enable floating wind turbines to become cheaper, as the wide range of possible design parameters and environmental conditions restricts designers ability to fully optimise the initial design; current simulation tools run at about real-time CPU speed, but many long simulations are needed to capture low-frequency behaviour. For example, approximate calculation models enabled automatic optimisation of a wide range of floating wind turbine designs by Hall et al.[11] Matha et al.[12] show that approximate models can be used to identify the critical design load cases to focus attention on. In both cases, exact results are not expected, but sufficient accuracy is needed that attention is focused in the right area of the design space or the right subset of load cases.

There are three main approaches to approximate modelling of floating wind turbines: (1) neglecting couplings between subsystems, (2) reduced-order nonlinear models and (3) linearised frequency-domain analysis.

Neglecting couplings between different aspects of the floating wind turbine allows for faster simulations, but there is a risk of missing important behaviour. For example, Nielsen et al.[1] found that the interaction between the control system and the floating platform dynamics creates an instability, while Jonkman[13] identified a platform yaw instability caused by a failed blade. Bae et al.[14] found that a simple drag-law model of the rotor loads, neglecting coupling to platform motion and the control system, overpredicted the platform motions, while Karimirad and Moan[15] found that a similar model with the coupling included gave better results. On the other hand, some couplings can reasonably be neglected, such as the nonlinear inertial coupling between platform motion and the rotor dynamics[16] and gyroscopic effects.[17]

The second type of approach is to retain the relevant couplings but simplify the model by omitting less important degrees of freedom. For example, Sandner et al.[18] describe such as reduced-order model of a floating wind turbine, and Sandner et al.[19] further reduce the degrees of freedom to focus on coupling the floating platform and controller designs. Matha et al.[4] compare the results of the reduced-order model across a range of design load cases to full nonlinear simulations.

The third type of approach, linearised frequency-domain analysis, is very computationally efficient, but the accuracy of the results depends on the accuracy of the linearised approximation of the true nonlinear behaviour. This approach has been used for modelling stall-regulated turbines,[20,21] offshore turbines[22] and initial design of foundations[23] and blades.[24] For floating turbines, it has been used to study a wide space of possible concepts,[10,11,25] to test the effect of wave energy converters on spar platforms,[26] and for controller design.[27]

The ways that the linearised approximation is constructed can be divided into two main families. Most common are *tangent linearisations*, which look locally at the behaviour of the nonlinear system about a mean operating point. This can be achieved through numerical perturbation of a full nonlinear model such as FAST,[28] or by analytical linearisation of the aerodynamic forces.[29] This linearisation works well when the system state remains close to the linearisation point (either because the nonlinear behaviour is weak, or because the perturbation in operating conditions are small). For example, Hall et al.[11] used this approach to represent the aerodynamic loads and mooring line stiffness in their optimisation model.

An alternative method of linearisation is a form of 'equivalent linearisation', which rather than looking at the nonlinear system's behaviour locally around one operating point aims to minimise the expected error of the linearisation over the range of operating conditions being considered.[30] Within this general approach, 'harmonic linearisation' and 'stochastic linearisation' apply to deterministic and stochastic situations, respectively. Stochastic linearisation has long been applied to modelling the nonlinear viscous drag forces on floating structures[31] and was applied to fixed wind turbines by Savenije and Peeringa[32] and to floating wind turbines by Hall et al.,[11] Lupton[33] and more recently by Lemmer et al.[34] to tailor the linearisation of the hydrodynamic loads to different sea states. Lupton and Langley[35] showed that harmonic linearisation can also give improved linearised models of the aerodynamic loads on the wind turbine rotor, and it can also be applied to capture a large part of the nonlinear control system behaviour, although in some operating conditions, the response is so nonlinear that it was not satisfactorily modelled. Pegalajar-Jurado et al.[10] present a method for linearised aerodynamic damping coefficients involving averaging values from multiple time-domain decay simulations, weighted by the probability distribution of wind speed. While this is not formulated as stochastic linearisation, it shares the general motivating principle.

Compared to a tangent linearisation method, the advantage of equivalent linearisation is to increase accuracy but at the cost of potentially greater computational requirements and complexity (though still an improvement over the full nonlinear time domain simulation). In some cases, equivalent linearisation can be carried out analytically, such as for the viscous drag forces in Morison's equation.[36] Lupton and Langley[35] instead found the equivalent linearisation from numerical evaluation of the nonlinear aerodynamic loads over a cycle of state variations. Generally, an iterative solution is needed since the equivalent linearisation depends on the system response, which in turn depends on the linearisation.

In summary, while equivalent linearisation has benefits over tangent linearisation for improved accuracy in modelling aerodynamic loading on wind turbines in isolation, it has not been shown how this can be applied to modelling a complete floating wind turbine system, including the coupled dynamics of aerodynamic and hydrodynamic loads together with the control system and structural dynamics. The main idea of this paper is to embed the linearised models of aerodynamic loads and control system behaviour presented in Lupton and Langley[35] in the context of a

complete model of a floating wind turbine. Our objective is to quantify the accuracy of this method over a range of operating conditions and, in cases where the accuracy is unsatisfactory, to diagnose the cause of the inaccuracy. Ultimately, the aim is to give improved estimates of key response variables under realistic stochastic wave and wind environments, to guide early-stage design optimisation. However, to give greater clarity on how the linearisation performs and the sources of errors, in this paper, we focus on only deterministic harmonic wind and wave inputs. In a frequency-domain model, this can be later generalised to arbitrary wind and wave spectra.

We begin by introducing the coupled nonlinear aero-hydro-servo-elastic model of the floating wind turbine which forms the basis for this study (Section 2), before deriving the harmonic and tangent linearised forms of the model (Section 3). Nonlinear time-domain simulations were run using a Bladed model of the OC3-Hywind turbine[37] to act as a reference, over a range of wind and sea conditions (Section 4). We assess the overall accuracy and simulation time of the linearised models (Section 5), before digging into the details to identify the causes behind specific cases where the linearised model performs less well (Section 6). This leads to conclusions about the performance of the linearised method and how it could be further improved in the future (Section 7).

2 | COUPLED AERO-HYDRO-SERVO-ELASTIC MODEL

The underlying coupled model of the floating wind turbine studied in this paper includes rigid-body motion of the floating platform, tower and blade flexibility and the pitch and torque controller behaviour. Aerodynamic loads are applied to the rotor, and mooring and hydrodynamic wave loads are applied to the floating structure. The model is initially formulated generally and later used to obtain results for the OC3-Hywind turbine[37] specifically.

In the time domain, the model equations can be written using the Cummins equation[38] as

$$(\boldsymbol{M}+\boldsymbol{A}_{\infty})\ddot{\boldsymbol{q}}(t)+\int_{-\infty}^{t}\boldsymbol{K}(t-\tau)\dot{\boldsymbol{q}}(\tau)d\tau+\boldsymbol{B}\dot{\boldsymbol{q}}(t)+\boldsymbol{C}\boldsymbol{q}(t)=\boldsymbol{Q}(\boldsymbol{q},t), \tag{1}$$

where $\boldsymbol{q}(t)$ are the system responses in generalised coordinates. $\boldsymbol{M}$, $\boldsymbol{B}$ and $\boldsymbol{C}$ are the mass, damping and stiffness matrices, whose components are defined in the following subsections. $\boldsymbol{A}_{\infty}$ is the hydrodynamic added mass matrix at infinite frequency, and $\boldsymbol{K}(t-\tau)$ is the radiation impulse response function. The generalised forces $\boldsymbol{Q}(\boldsymbol{q},t)$ consist of variable contributions from wind and waves and the constant weight of the mooring lines:

$$\boldsymbol{Q}(\boldsymbol{q},t)=\boldsymbol{Q}_{\text{hydro}}(t)+\boldsymbol{Q}_{\text{wind}}(\boldsymbol{q},t)+\boldsymbol{Q}_{\text{mooring}}. \tag{2}$$

Here, $\boldsymbol{Q}_{\text{wind}}(\boldsymbol{q},t)$ includes all components of the aerodynamic forces, including aerodynamic damping. In addition, there are equations governing the control system states. These, and the origin of the terms above, are explained in the following sections.

2.1 | Structural model

The flexible structure is modelled with six degrees of freedom: one normal mode per blade, two tower fore-aft attachment modes (i.e., modes allowing translation and rotation of the tower top), the rotor rotation, and three rigid-body platform motions—surge (fore-aft translation), heave (vertical translation) and pitch (rotation about the transverse axis). The rotor rotation is prescribed in some simulations but free to vary in the simulations with the control system included. In addition, the blade pitch joints are modelled but always given prescribed rotations.

The structural matrices are found by building a multibody structural model (Figure 1) using the *mbwind* framework[39] developed by Lupton,[33] with the parameters for the OC3-Hywind turbine specified by Jonkman.[37] From this multibody model, the matrices $\boldsymbol{M}_{\text{struct}}$, $\boldsymbol{B}_{\text{struct}}$ and $\boldsymbol{C}_{\text{struct}}$ are found by numerical linearisation. In this case, tangent linearisation gives sufficient accuracy as nonlinear dynamic effects are small.[16]

Because the rotor is rotating, the multiblade coordinate (MBC) or Coleman transformation[40] is applied to the blade degrees of freedom, after the linearised matrices are found, so that the blade deflections are transformed into a nonrotating frame of reference. For example, the flapwise deflection of blade k is expressed as

$$\alpha_k=a_0+a_1\cos\psi_k+b_1\sin\psi_k, \tag{3}$$

where for a three-bladed rotor, the azimuth of blade k is $\psi_k(t)=\psi(t)+2\pi(k-1)/3$, in which ψ is the rotor azimuth and a_0, a_1 and b_1 are the 'MBCs'. In this case, a_0 represents the average flapwise deflection across all three blades, while a_1 and b_1 represent tilt and yaw motions, respectively. Edgewise deflections are described similarly.

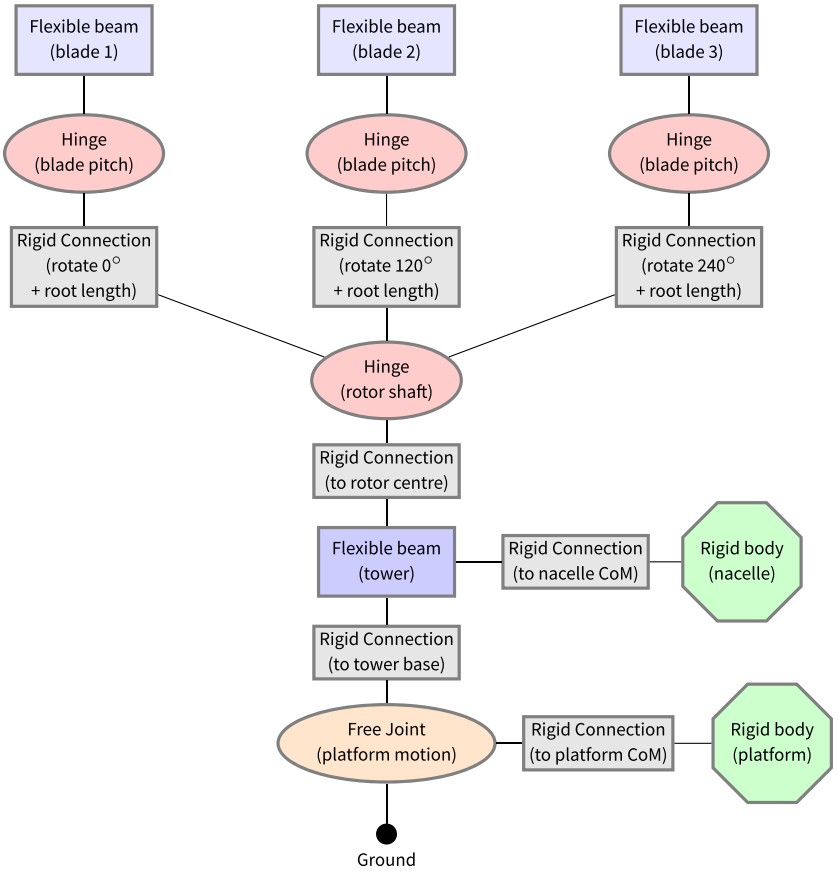

FIGURE 1 Elements making up the multibody model of the flexible floating wind turbine. The free joint defines the position and orientation of the platform origin, located at the mean water level. The bottom of the flexible part of the tower and the centre of mass of the platform are offset from this origin by rigid connections. The 'nacelle' contains the gearbox, bearings and generator at the tower top. 'Root length' refers to the radial distance from the rotor axis to the start of the flexible blade. The blades are modelled with a Euler–Bernoulli beam model, accounting for blade twist (see Lupton[33] for details)

In practice, the MBC transformation between the blade-fixed coordinates $\boldsymbol{y}$ and the fixed-frame coordinates $\boldsymbol{z}$ is achieved via a transformation matrix,

$$\boldsymbol{y} = \boldsymbol{B}(t)\boldsymbol{z}, \tag{4}$$

where

$$\boldsymbol{B}(t) = \begin{bmatrix} \boldsymbol{I}_N & \boldsymbol{I}_N \cos\psi_1 & \boldsymbol{I}_N \sin\psi_1 \\ \boldsymbol{I}_N & \boldsymbol{I}_N \cos\psi_2 & \boldsymbol{I}_N \sin\psi_2 \\ \boldsymbol{I}_N & \boldsymbol{I}_N \cos\psi_3 & \boldsymbol{I}_N \sin\psi_3 \end{bmatrix}, \tag{5}$$

in which $\boldsymbol{I}_N$ is an identity matrix of size N and N is the number of degrees of freedom of each blade. After solving the response in terms of the fixed-frame coordinates $\boldsymbol{z}$, the blade response is recovered by the reverse transformation.

2.2 | Hydrodynamic and mooring system loads

Linear hydrodynamic loads are applied to the platform. Wave excitation loads are assumed to be due to regular linear waves, which are aligned with the rotor and the wind direction. Although in practice, second-order nonlinear hydrodynamic forces may be important, they are not included here as they are known to be feasible to include in frequency-domain analysis[41] but would add significant computational expense to the time-domain reference results.

In reality, flow separation is likely to occur in large waves over part of the spar, so strictly viscous drag forces should be included.[37] However, for simplicity in comparing the accuracy of the linearisation itself, they have been neglected in both the nonlinear reference simulations and in the linearised models.

Therefore, the linear wave excitation at frequency ω_2 is

$$\boldsymbol{Q}_{\text{hydro}}(t) = \rho g V_0 \boldsymbol{l}_z + \boldsymbol{X}(\omega_2)\zeta \cos(\omega_2 t + \phi_2), \tag{6}$$

where ρ is the water density, V_0 is the displaced volume of the floating platform, $\boldsymbol{l}_z$ is a column of the identity matrix corresponding to the z-coordinate, $\boldsymbol{X}(\omega)$ is the frequency-dependent wave excitation force per unit wave amplitude and ζ is the wave amplitude.

The linear hydrodynamic matrices and the mooring line stiffness $\boldsymbol{C}_{\text{mooring}}$ and weight $\boldsymbol{Q}_{\text{mooring}}$ are supplied for the case study floating platform by Jonkman.[37]

2.3 | Aerodynamic loads

Wind loads are calculated using a blade element momentum (BEM) model. The wind speed is assumed to be uniform across the whole rotor, with harmonic variations in wind speed, using the same approach described by Lupton and Langley.[35] For simplicity, the wake dynamics are not included here, as they are only weakly nonlinear,[35] and so they do not affect the main focus on the effectiveness of the linearisation approach.

The force per unit length at each blade station radius r_i is calculated in the BEM model as

$$F_{\text{blade}}(r) = \text{BEM}(U, \Omega_r, \theta, \rho, w(r),\ v_{\text{blade}}(r)), \tag{7}$$

where U is the wind speed, Ω_r is the rotor speed, θ is the blade pitch angle, ρ is the air density, $\boldsymbol{w}(r_i)$ is the wake state at station i and $\boldsymbol{v}_{\text{blade}}(r_i)$ is the instantaneous velocity of the blade itself. For simplicity, in this study, the variations around the rotor are neglected and this velocity is calculated based on the average blade motion across the rotor:

$$v_{\text{blade}}(r) = v_{\text{hub}} + \frac{1}{3}\sum_{b=1}^{3} v_b(r).$$

This means that the differential effect of platform pitching on individual blade velocities is not included, but the error introduced by this simplification is insignificant compared to the other differences between the nonlinear and linear models.

The blade loads are numerically integrated to give the loading on the hub and the flexible blades, which is projected into the generalised coordinates of the multibody structural model[33] to give the generalised forces $\boldsymbol{Q}_{\text{aero}}(\boldsymbol{x})$ as follows. The rotor loads are

$$\boldsymbol{F}_{\text{rotor}} = 3\int \boldsymbol{F}_{\text{blade}}(r)\,\text{d}r \tag{8}$$

$$\boldsymbol{M}_{\text{rotor}} = 3\int r\boldsymbol{k} \times \boldsymbol{F}_{\text{blade}}(r)\,\text{d}r, \tag{9}$$

where $\boldsymbol{k}$ is a unit vector pointing along the blade. These loads are assumed to act perpendicular to the rotor plane, so they are rotated through the platform pitch angle $\phi(t)$ to give the forces and moments applied at the hub in the fixed coordinate system $\boldsymbol{F}_{\text{hub}}$ and $\boldsymbol{M}_{\text{hub}}$. Finally, these forces and moments are projected into the generalised coordinates of the multibody structural model[33] to give the generalised forces:

$$\boldsymbol{Q}_{\text{aero}}(x) = \boldsymbol{R}_{F,\text{hub}}\boldsymbol{F}_{\text{hub}} + \boldsymbol{R}_{M,\text{hub}}\boldsymbol{M}_{\text{hub}} + \sum_i \boldsymbol{R}_{F,\text{blade}}(r_i)\boldsymbol{F}_{\text{blade}}(r_i), \tag{10}$$

where $\boldsymbol{R}_{F,\text{hub}}$ and $\boldsymbol{R}_{M,\text{hub}}$ are projection matrices for forces and moments applied at the hub and $\boldsymbol{R}_{F,\text{blade}}(r_i)$ is the projection matrix into the modal stress of the flexible blade for a force applied to blade station i. Because the forces are assumed to act symmetrically across the rotor, this projection matrix maps the forces into the first (symmetric) coordinate of the MBC-transformed blade coordinates (Section 2.1). These projection matrices depend on the structural state $\boldsymbol{q}(t)$.

The calculation of the aerodynamic loads is implemented using the open source Python package *bemused*[42] developed by Lupton.[33]

2.4 | Control system

The generator torque and blade pitch control systems were modelled as previously described by Lupton and Langley,[35] based on the controller implementation supplied for the OC3-Hywind turbine,[43] with the OC3 modifications to avoid instabilities included.

The aim of the torque controller is to maintain the optimum rotor speed which leads to the correct air flow for maximum aerodynamic efficiency. The torque demand is based on the filtered generator speed

$$\dot{\Omega}_g(t) = \omega_c(G\Omega_r(t) - \Omega_g(t)), \tag{11}$$

where G is the gearbox ratio, $\Omega_r(t)$ is the rotor speed and ω_c is the corner frequency of the filter. At high enough wind speeds that the rated power P_{rated} is being produced, the torque controller switches to constant torque mode, and the pitch controller becomes active. To prevent the controllers conflicting, the torque controller is forced into constant torque mode whenever the pitch angle θ is greater than some minimum value θ_{CP}. Therefore, the demanded generator torque is given by

$$Q_g = \begin{cases} f(\Omega_g) & \text{when } \theta \le \theta_{\text{CP}} \\ P_{\text{rated}}/\Omega_{\text{rated}} & \text{otherwise.} \end{cases} \tag{12}$$

The response of the rotor speed is governed by the drive train equation

$$J\dot{\Omega}(t) = Q_{\text{aero}}(t) - GQ_g(t), \tag{13}$$

where J is the rotational inertia of the rotor and $Q_{\text{aero}}(t)$ is the aerodynamic torque determined as described in Section 2.3.

The pitch controller is based on a PI controller acting on the error between the filtered generator speed $\Omega_g(t)$ and the nominal rated generator speed Ω_{rated}. The demanded pitch angle is

$$\theta(t) = G_K(t)[K_P(\Omega_g(t) - \Omega_{\text{rated}}) + K_I I_\epsilon(t)], \tag{14}$$

where K_P and K_I are the proportional and integral gains, respectively, and $I_\epsilon(t)$ is the integral error state. The factor $G_K(t)$ represents a 'gain schedule', which compensates for the variable sensitivity of the blade loads to changes in pitch angle at different wind speeds, determined by the pitch angle:

$$G_K(t) = \frac{1}{1 + \theta(t)/\theta_2}, \tag{15}$$

where θ_2 is the pitch angle at which the gain should be halved. The pitch controller is automatically deactivated when $\Omega_g(t) < \Omega_{\text{rated}}$ because then the error is negative, forcing the pitch angle to zero and preventing conflict with the torque controller. The pitch controller integral state is governed by

$$\dot{I}_\epsilon(t) = \Omega_g(t) - \Omega_{\text{rated}}. \tag{16}$$

3 | LINEARISATION

The nonlinear excitation forces due to the aerodynamics and the nonlinear control system behaviour described in Section 2 now need to be linearised. For simplicity, the other parts of the model (i.e., the hydrodynamic and mooring loads) are here already given in a linear form, but in general, other effects such as nonlinear mooring forces could also be dealt with similarly. Unlike the harmonic linearisation approach presented in Lupton and Langley,[35] the floating wind turbine is now subject to both wind and wave loading at different frequencies. For a general nonlinear function $f(x,\dot{x})$, the aim therefore is to produce a good approximation of the output of $\boldsymbol{f}$ given harmonic variations in the inputs $\boldsymbol{x}$ at frequencies ω_1 and ω_2. This can be conveniently written in terms of complex exponentials as

$$x(t) = x_0 + \frac{1}{2}\left(x_1 e^{i\omega_1 t} + x_1^* e^{-i\omega_1 t}\right) + \frac{1}{2}\left(x_2 e^{i\omega_2 t} + x_2^* e^{-i\omega_2 t}\right), \tag{17}$$

where $\boldsymbol{x}_0$ is the mean value of $\boldsymbol{x}$, $\boldsymbol{x}_1$ and $\boldsymbol{x}_2$ are complex vectors representing the magnitude and phase of $\boldsymbol{x}$ at frequencies ω_1 and ω_2 and x_1^* and x_2^* are their complex conjugates. The nonlinear response is not necessarily harmonic but can be written similarly as

$$\boldsymbol{f}(t) = \boldsymbol{f}_0 + \frac{1}{2}\left(\boldsymbol{f}_1 e^{i\omega_1 t} + \boldsymbol{f}_1^* e^{-i\omega_1 t}\right) + \frac{1}{2}\left(\boldsymbol{f}_2 e^{i\omega_2 t} + \boldsymbol{f}_2^* e^{-i\omega_2 t}\right) + \boldsymbol{\epsilon}(t), \tag{18}$$

where $\boldsymbol{\epsilon}(t)$ represents higher harmonics in $\boldsymbol{f}(t)$ at frequency $n\omega_i$, $i = 1, 2$, $n > 1$, which are neglected in the linearised model.

Because the harmonic approximation depends on the response, an iterative solution is required which is set out in Sections 3.1–3.3.

3.1 | Harmonic state variables and inputs

The complete vector of inputs and state variables for the model is

$$\boldsymbol{x}(t) = \begin{bmatrix} \boldsymbol{u}(t) \\ \boldsymbol{q}(t) \\ \boldsymbol{z}(t) \end{bmatrix}, \tag{19}$$

where $u(t) = [U(t)\,\Omega_r(t)\,\theta(t)\,\eta(t)]^{\mathsf{T}}$ are the prescribed inputs of wind speed U, rotor speed Ω_r, blade pitch angle θ and wave height η; $\boldsymbol{q}(t)$ are the structural states discussed in Section 2.1; and $\boldsymbol{z}(t)$ are the control system states discussed in Section 2.4. When the control system is included in the model, the rotor speed Ω_r and blade pitch angle θ are removed from the list of prescribed inputs as they are controlled directly. Note that dynamic wake states could be included in addition[35] within $\boldsymbol{x}(t)$, but for simplicity, a frozen wake model is used here.

The prescribed inputs are set at frequencies ω_1 and ω_2 corresponding to the wind and wave frequencies according to Equation (17):

$$\boldsymbol{u}_0 = \begin{bmatrix} U_0 \\ \Omega_{r,0} \\ \theta_0 \\ 0 \end{bmatrix} \qquad \boldsymbol{u}_1 = \begin{bmatrix} \Delta U \\ 0 \\ 0 \\ 0 \end{bmatrix} \qquad \boldsymbol{u}_2 = \begin{bmatrix} 0 \\ 0 \\ 0 \\ \zeta \end{bmatrix}. \tag{20}$$

That is, only $U(t)$ includes harmonic variation at frequency ω_1, and only $\eta(t)$ includes harmonic variation at frequency ω_2.

The components of the state variables $\boldsymbol{q}(t)$ and $\boldsymbol{z}(t)$ at each frequency are unknowns which will be solved next.

3.2 | Linearised forces

The nonlinear functions introduced in Sections 2.3 and 2.4 are next replaced by the harmonic approximation in Equation (18). The coefficients in that equation are found as[44]

$$\boldsymbol{f}_0^{\text{har}} = \frac{1}{T}\int_0^T \boldsymbol{f}[\boldsymbol{x}(t), \dot{\boldsymbol{x}}(t)]\,\mathrm{d}t, \tag{21a}$$

$$\boldsymbol{f}_1^{\text{har}} = \frac{2}{T}\int_0^T \boldsymbol{f}[\boldsymbol{x}(t), \dot{\boldsymbol{x}}(t)] e^{-i\omega_1 t}\,\mathrm{d}t, \tag{21b}$$

$$\boldsymbol{f}_2^{\text{har}} = \frac{2}{T}\int_0^T \boldsymbol{f}[\boldsymbol{x}(t), \dot{\boldsymbol{x}}(t)] e^{-i\omega_2 t}\,\mathrm{d}t. \tag{21c}$$

In practice, these harmonics are calculated using a fast Fourier transform (FFT). Since harmonics at two frequencies (representing the wave and the wind) are included in the input, the nonlinear functions must be evaluated over several periods in the time domain to be able to resolve the corresponding harmonic components in the output of the nonlinear functions. More generally, additional harmonic components could be included in the same way. The response to random rather than harmonic inputs is also generally of interest, in which case the equivalent linearisation is based on the expected value of the nonlinear function.[30] While the insights gained through studying the harmonic linearisation are also relevant to the stochastic case, the details of how this could be applied to model floating wind turbines have yet to be demonstrated.

Specifically, to find the linearised aerodynamic loads, the nonlinear loads $\boldsymbol{Q}_{\text{aero}}(\boldsymbol{x})$ are evaluated for a sample of points over the harmonic variation in $\boldsymbol{x}$ specified by Equation (19), before applying a FFT to obtain the coefficients in Equation (21), which in this case are $\boldsymbol{Q}_{\text{aero, 0}}$, $\boldsymbol{Q}_{\text{aero, 1}}$ and $\boldsymbol{Q}_{\text{aero, 2}}$.

Since here only linear hydrodynamic loading is included, the harmonic components of $\boldsymbol{Q}_{\text{hydro}}(t)$ from Equation (6) can be written directly as

$$\boldsymbol{Q}_{\text{hydro,0}} = \rho g V_0 \boldsymbol{l}_z \qquad \boldsymbol{Q}_{\text{hydro,1}} = 0 \qquad \boldsymbol{Q}_{\text{hydro,2}} = \boldsymbol{X}(\omega_2)\zeta. \tag{22}$$

Nonlinear hydrodynamic loads could be included in a similar way to the nonlinear aerodynamic loads.

3.3 | Linearised harmonic solution

Now that the forces have been expressed as harmonic components, the equation of motion Equation (1) can be transformed into the frequency domain and solved. The frequency domain equivalent is

$$\left[-\omega^2 \boldsymbol{M}(\omega) + i\omega \boldsymbol{B}(\omega) + \boldsymbol{C}\right]\boldsymbol{q}(\omega) = \boldsymbol{Q}(\omega), \tag{23}$$

where

$$\boldsymbol{M}(\omega) = \boldsymbol{M}_{\text{struct}} + \boldsymbol{A}_{\text{hydro}}(\omega) \tag{24a}$$

$$\boldsymbol{B}(\omega) = \boldsymbol{B}_{\text{struct}} + \boldsymbol{B}_{\text{hydro}}(\omega) \tag{24b}$$

$$\boldsymbol{C} = \boldsymbol{C}_{\text{struct}} + \boldsymbol{C}_{\text{hydro}} + \boldsymbol{C}_{\text{mooring}}. \tag{24c}$$

To find the structural response, the linearised loads are projected into the generalised coordinates of the system using a projection matrix supplied by the multibody model.[33] The system transfer function is evaluated to find the static response and at the two harmonic frequencies:

$$\boldsymbol{H}_0 = [\boldsymbol{C}]^{-1} \tag{25a}$$

$$\boldsymbol{H}_1 = \left[-\omega_1^2 \boldsymbol{M}(\omega_1) + i\omega_1 \boldsymbol{B}(\omega_1) + \boldsymbol{C}\right]^{-1} \tag{25b}$$

$$\boldsymbol{H}_2 = \left[-\omega_2^2 \boldsymbol{M}(\omega_2) + i\omega_2 \boldsymbol{B}(\omega_2) + \boldsymbol{C}\right]^{-1}. \tag{25c}$$

The components of the harmonic response, corresponding to Equation (17) above, are found as

$$\boldsymbol{q}_j = \boldsymbol{H}_j \boldsymbol{Q}_j \qquad j = 0, 1, 2, \tag{26}$$

where $\boldsymbol{Q}_0$ are the mean generalised forces and $\boldsymbol{Q}_1$ and $\boldsymbol{Q}_2$ are the frequency-domain components of the generalised forces at ω_1 and ω_2 obtained from Equations (21) and (22). Since the generalised forces are nonlinear functions of the response, the solution is found numerically by solving the nonlinear equations

$$0 = \boldsymbol{q}_j - \boldsymbol{H}_j \boldsymbol{Q}_j(\boldsymbol{q}_0, \boldsymbol{q}_1, \boldsymbol{q}_2) \qquad j = 0, 1, 2. \tag{27}$$

The initial guess for $\boldsymbol{q}_j$ is obtained from the tangent linearisation solution, described in the following section. The solution is found using a standard multidimensional root-finding algorithm.[45]

In addition to the structural response, the linearised control system response must also be found by solving the following nonlinear equations in parallel with Equation (27). The rotor speed dynamic response (Equation 13) is determined by

$$0 = (Q_a)_0 - G(Q_g)_0 \tag{28a}$$

$$(\Omega)_1 = \left[(Q_a)_1 - G\left(Q_g\right)_1\right]/Ji\omega_1 \tag{28b}$$

$$(\Omega)_2 = \left[(Q_a)_2 - G\left(Q_g\right)_2\right]/Ji\omega_2. \tag{28c}$$

The filtered generator speed Ω_g is determined by

$$(\Omega_g)_0 = G(\Omega)_0 \tag{29a}$$

$$(\Omega_g)_1 = \frac{G(\Omega)_1}{1 + i\omega_1/\omega_c} \tag{29b}$$

$$(\Omega_g)_2 = \frac{G(\Omega)_2}{1 + i\omega_2/\omega_c}, \tag{29c}$$

while the linearised solution of Equation (16) is determined by

$$0 = (\Omega_g)_0 - \Omega_{\text{rated}} \tag{30a}$$

$$(l_\epsilon)_1 = \left[(\Omega_g)_1\right]/i\omega_1 \tag{30b}$$

$$(l_\epsilon)_2 = \left[(\Omega_g)_2\right]/i\omega_2. \tag{30c}$$

Below the rated wind speed, when the pitch controller is not active, Equations (27)–(29) are solved simultaneously. Above the rated wind speed, the pitch controller is active and Equation (30) is solved in addition.

3.4 | Linearised tangent solution

To understand if the extra effort of finding the iterative harmonic linearisation solution is worthwhile, the tangent linearisation solution was also found. This is calculated in a similar way to the harmonic linearised solution: the structural model and wave loads are identical. The difference is in the linearisation of the aerodynamic loads, which are found by perturbing the wind speed and platform motion about the mean operating point.

The solution is found by solving for the mean value and the amplitudes of the two harmonics, as in Equation (26), but now with the transfer functions identified as

$$\boldsymbol{H}_0 = [\boldsymbol{K}]^{-1} \tag{31a}$$

$$\boldsymbol{H}_1 = \left[-\omega_1^2\boldsymbol{M}(\omega_1) + i\omega_1(\boldsymbol{C}(\omega_1) + \boldsymbol{C}_q) + (\boldsymbol{K} + \boldsymbol{K}_q)\right]^{-1} \tag{31b}$$

$$\boldsymbol{H}_2 = \left[-\omega_2^2\boldsymbol{M}(\omega_2) + i\omega_2(\boldsymbol{C}(\omega_2) + \boldsymbol{C}_q) + (\boldsymbol{K} + \boldsymbol{K}_q)\right]^{-1}. \tag{31c}$$

Here, $\boldsymbol{M}$, $\boldsymbol{C}$ and $\boldsymbol{K}$ are the same system matrices which appear in Equation (25). $\boldsymbol{C}_q$ and $\boldsymbol{K}_q$ are the parts of the linearised aerodynamic force which depend on the platform motion and blade vibration, thereby accounting approximately for aeroelastic effects.

The components of the generalised forces $\boldsymbol{Q}_j$ are

$$\boldsymbol{Q}_j^{\text{wind}} = \left(\boldsymbol{K}_U + i\omega_j\boldsymbol{C}_U\right)U_j \; j = 0, 1, 2 \tag{32a}$$

$$\boldsymbol{Q}_j^{\text{hydro}} = \rho g V_0 \boldsymbol{I}_z + \boldsymbol{X}(\omega)\zeta_j \tag{32b}$$

$\boldsymbol{C}_U$ and $\boldsymbol{K}_U$ are the parts of the linearised aerodynamic force which depend on the wind speed. U_0, U_1 and U_2 are the mean wind speed and the amplitudes of the wind speed variation occurring at frequencies ω_1 and ω_2, respectively. ζ_0, ζ_1 and ζ_2 are similarly the components of the

wave heights. Since ω_1 is the wind loading frequency and ω_2 is the wave loading frequency, in fact, $U_2 = 0$ and $\zeta_0 = \zeta_1 = 0$. The mooring forces are not shown here as they are defined directly by the linear stiffness $\boldsymbol{C}_{\text{mooring}}$ (although if the mooring force was nonlinear, it could be linearised similarly to the wind loads).

Note that because the nonlinear force is numerically linearised, the 'stiffness' and 'damping' components of the force do not need to be explicitly found in the harmonic linearisation (Equation 25). In contrast, in the tangent linearisation, these stiffness and damping matrices are identified explicitly and included in the transfer function matrices (Equations 31 and 32).

4 | REFERENCE SIMULATIONS

The accuracy of the linearised model is tested in two stages. First, the response is tested for constant rotor speed and blade pitch angle, over a wide range of wind and wave conditions, comparing the harmonic linearisation, tangent linearisation and nonlinear reference results from Bladed. Then, the overall response is tested, including the control system behaviour, for a more limited set of conditions, comparing the harmonic linearisation to the nonlinear results.

4.1 | Wind and wave conditions to test

The wind and wave conditions tested are shown in Table 1. The intention of including two smaller wave heights was to exercise the linearisation of the nonlinear part of the loading: since in the present model, the aerodynamic loads are nonlinear while the hydrodynamic loads are linear, it might be expected that the worst case for the linearised model would be the small waves. In practice, this is not always the case because it was not possible to limit the hydrodynamic loading in Bladed to a purely linear model, as described below. The large 25-m waves are included to represent an extreme sea state. The wave heights and periods were selected from the typical North Sea scatter table provided by Faltinsen.[41] The wind conditions were chosen to represent operation both below and above the rated wind speed. The frequencies chosen for the wind speed variations include values from across the range that could be relevant, from the platform natural frequencies up to near the frequency of the 'extreme operating gust'.[46]

In the second stage, when the control system is included in the model, results are obtained for one set of wave conditions (T = 10 s, H = 6 m) and for harmonic wind with a frequency of $\omega = 0.32$ rad s^{-1} only.

4.2 | Bladed simulations

Simulations in Bladed (version 4.1) were run for 2,000 s to ensure that transient platform motions have decayed.

For practical reasons, more degrees of freedom were included in the simulations than in the linearised model, but this does not affect the results: because in Bladed, modes must be included in sequence, to reach the tower fore-aft rotation attachment mode, the side–side and torsion tower modes were also included. Also, it is not possible to exclude the platform sway, roll and yaw degrees of freedom, but no significant response was found in these directions.

Bladed has the capability to model individual mooring lines with nonlinear characteristics, but for comparison with the linearised results, a simple linear stiffness matrix was applied at the platform origin to represent the mooring lines. Mooring line damping was applied to represent the additional linear damping defined by OC3.

4.3 | Differences between Bladed model and nonlinear model

Because of limitations in the way the model can be set up in the Bladed software, there are a few reasons that the reference Bladed results do not exactly replicate the behaviour of the nonlinear model used here as the basis for linearisation, even before the linearisations are applied.

TABLE 1 Input parameters for simulations

Parameter	Symbol	Values
Mean wind speed	U	8 and 16 m s^{-1}
Wind variation amplitude	A	1, 2, 3, 4 and 5 m s^{-1}
Wind variation frequency	ω	0.10, 0.32 and 1.00 rad s^{-1}
Wave height and period	H, T	(1 m, 7 s), (6 m, 10 s), (25 m, 16 s)

Since the version of Bladed used could not make use of the hydrodynamic added mass, damping and wave excitation matrices (Section 2.2), the hydrodynamic loads in Bladed are calculated using Morison's equation. This is justified for this model because the diffraction and wave radiation effects are small.[37]

Even without the viscous drag forces, the hydrodynamic loads in Bladed are nonlinear, due to the use of Wheeler stretching to calculate the fluid velocity around the free surface.[9] In regular waves, this introduces an additional mean surge force which is not included in the linear model.

A subtle problem is created by the motion of the rotor through the air as the platform pitches. In the present work, the harmonic wind speed has been defined as a function of time, $U = A\cos\omega t$. In Bladed, the wind speed is defined as a spatial field, which moves past the rotor at the mean wind speed. An artificial wind field is defined containing sinusoidal variations in wind speed which would, if the rotor was stationary, result in the equivalent sinusoidal variation in wind speed at the rotor. However, as the rotor moves through this field, the wind speed measured at the rotor is no longer purely sinusoidal (Figure 2). Additional harmonics are therefore expected in the aerodynamic loads reported by Bladed, at the sum and difference of the wind and wave frequencies, as seen in the figure.

As discussed in Section 2.3, the linearised solutions provide the average response over the three blades. In the nonlinear simulation, the response is different between the three blades, due to the varying relative wind speed across the rotor. In the results presented here, the nonlinear blade responses are averaged for comparison with the linearised results.

4.4 | Basis for comparison

To reflect the agreement between the linearised and nonlinear results across all the combinations of conditions listed in Table 1, the error in the peak–peak range for five variables is used: the platform surge, heave and pitch, the tower translational deflection and the blade tip deflection. The peak–peak error is a simple measurement but is relevant whether extreme or fatigue loads are of interest. Because the structural model is linear, the error in the deflections is also indicative of the error in the structural bending moments and forces. The error is defined as

$$\epsilon_{PP} = \frac{|y_{PP} - z_{PP}|}{y_{PP}}, \tag{33}$$

where

$$\begin{aligned} y_{PP} &= \max(y) - \min(y) \\ z_{PP} &= \max(z) - \min(z), \end{aligned}$$

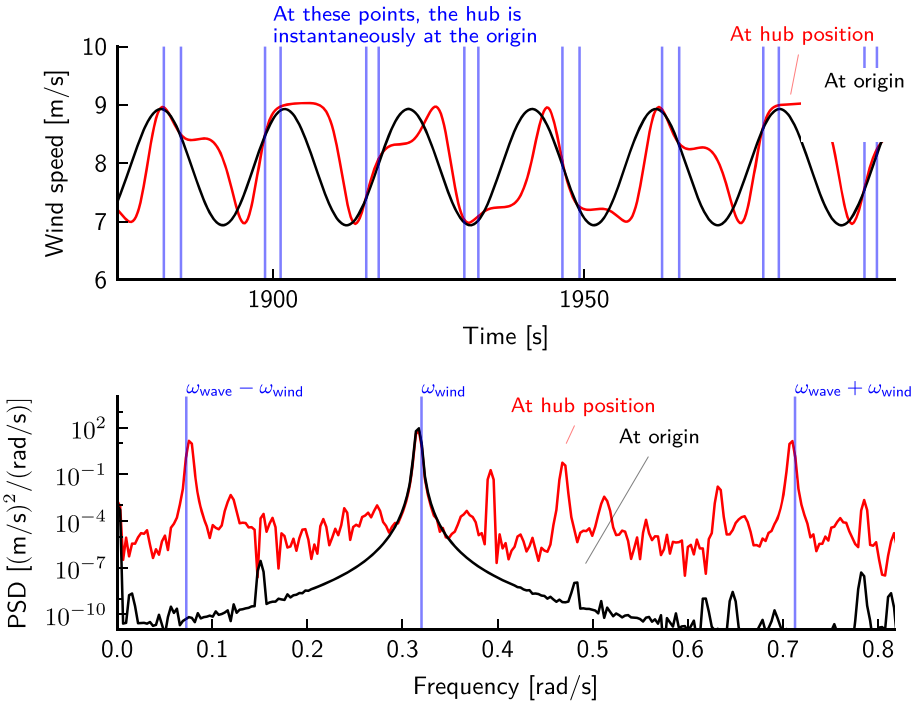

FIGURE 2 The wind speed in Bladed is defined as a spatial field which moves past the rotor. Top: time series of wind speed measured at the fixed origin and at the rotor hub. As the platform moves, the wind speed measured at the hub is not sinusoidal. Bottom: spectrum of wind speed measurements. Additional harmonics are seen at the sum and difference of the wind and wave frequencies when measured at the moving hub position

in which z is the linearised result and y is the nonlinear reference result.

The target accuracy will depend on the application of the linearised analysis. Previous examples include the following: Schløer et al.[47] describe fatigue damage errors of 8% as 'comparing well'; Matha et al.[12] found differences in extreme loads of about 5% between FAST and their reduced-order nonlinear model, with differences in fatigue damage of 25%; and Pegalajar-Jurado et al.[10] found errors in the largest response peaks of 4% to 12% and errors of up to 11% in fatigue damage. However, these are not all directly comparable as they are defined in different ways. For the sake of argument, here the accuracy is considered to be 'good' if the error is less than 5% and 'acceptable' if under 10%.

5 | RESULTS: OVERALL ACCURACY AND COMPUTATIONAL TIME

The accuracy of the linearised models is now assessed with reference to the Bladed simulation results. The overall errors are presented first for the case with fixed rotor speed and blade pitch angle and then with the control system behaviour. The harmonic and tangent linearisations are compared in accuracy and simulation time required. These headline results are then investigated in more detail in Section 6.

5.1 | Comparison of error (with fixed rotor speed and blade pitch angle)

The peak–peak error, normalised by the peak–peak amplitude of the nonlinear Bladed results (Section 4.4), is plotted for the full range of conditions in Figures 3–7. Each figure contains 12 contour plots, each showing the dependence of the error on the amplitude and frequency of the wind speed variations. The contour plots are arranged into columns corresponding to the three sea states and rows corresponding to the two mean wind speeds. The results for both the harmonic and tangent linearisations are given in each figure. For ease of comparison, a consistent colour scale is used in each figure showing errors from 0% to 20%. Larger errors are shown by additional contour lines.

The heave response (Figure 3) shows large relative errors. These occur when the wind loading is dominant (i.e., for 1-m waves and for the larger waves paired with the lower wind speeds). When the wave loads are dominant, the errors are lower. The causes of this will be investigated in more detail in Section 6.2.

The errors in the surge and pitch responses are shown in Figures 4 and 5. The behaviour of these two responses is broadly similar. Good accuracy is achieved for small variations in wind speed, with increasing peak–peak error for larger variations. Better accuracy is achieved with the mean wind speed of 16 m s^{-1} than with 8 m s^{-1}, and this is consistent with the results previously reported by Lupton and Langley[35] where weaker

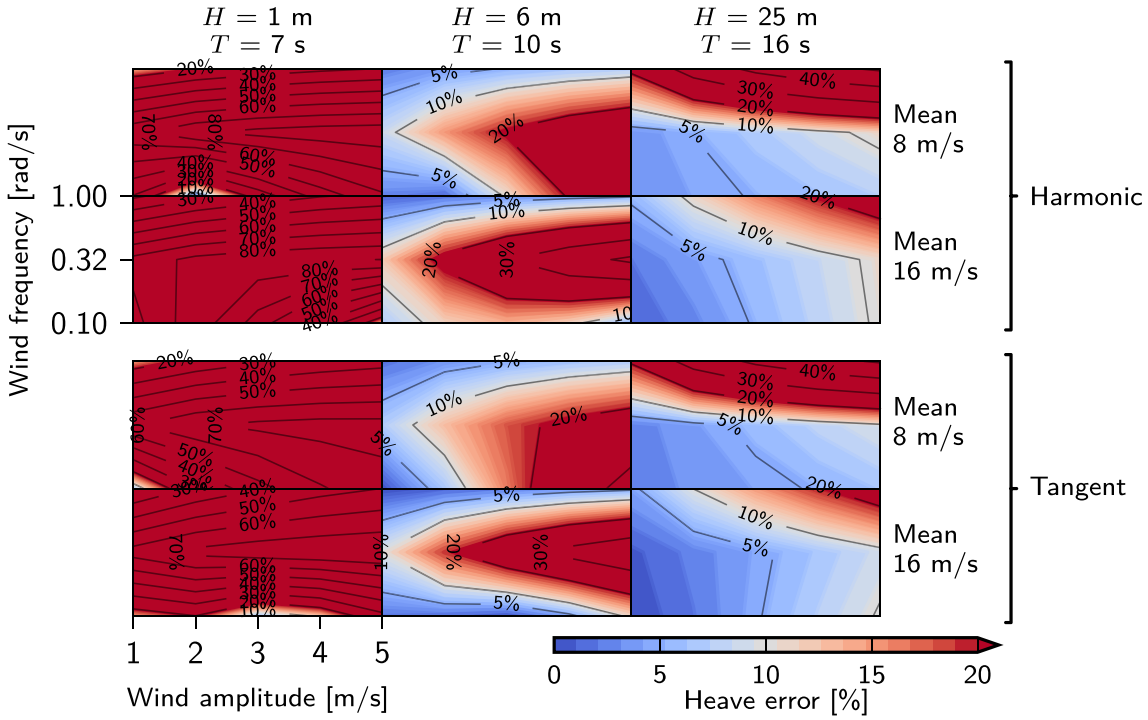

FIGURE 3 Normalised peak–peak error between nonlinear (Bladed) and harmonic solutions in heave response

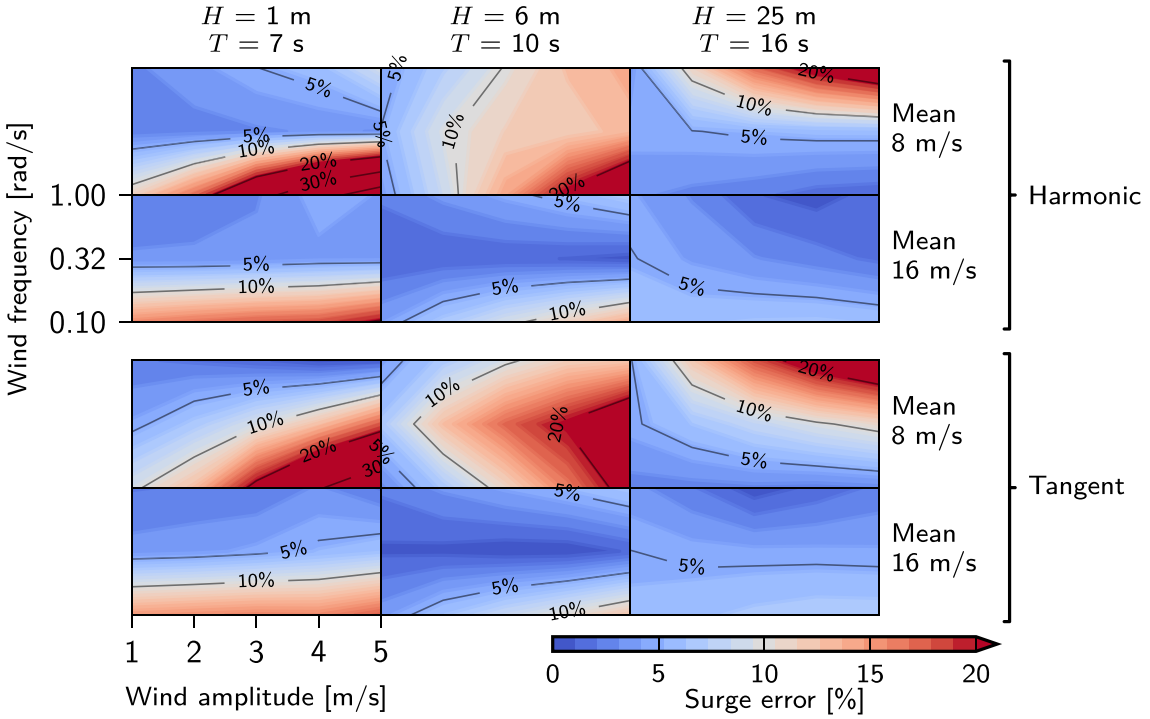

FIGURE 4 Normalised peak–peak error between nonlinear (Bladed) and harmonic solutions in surge response

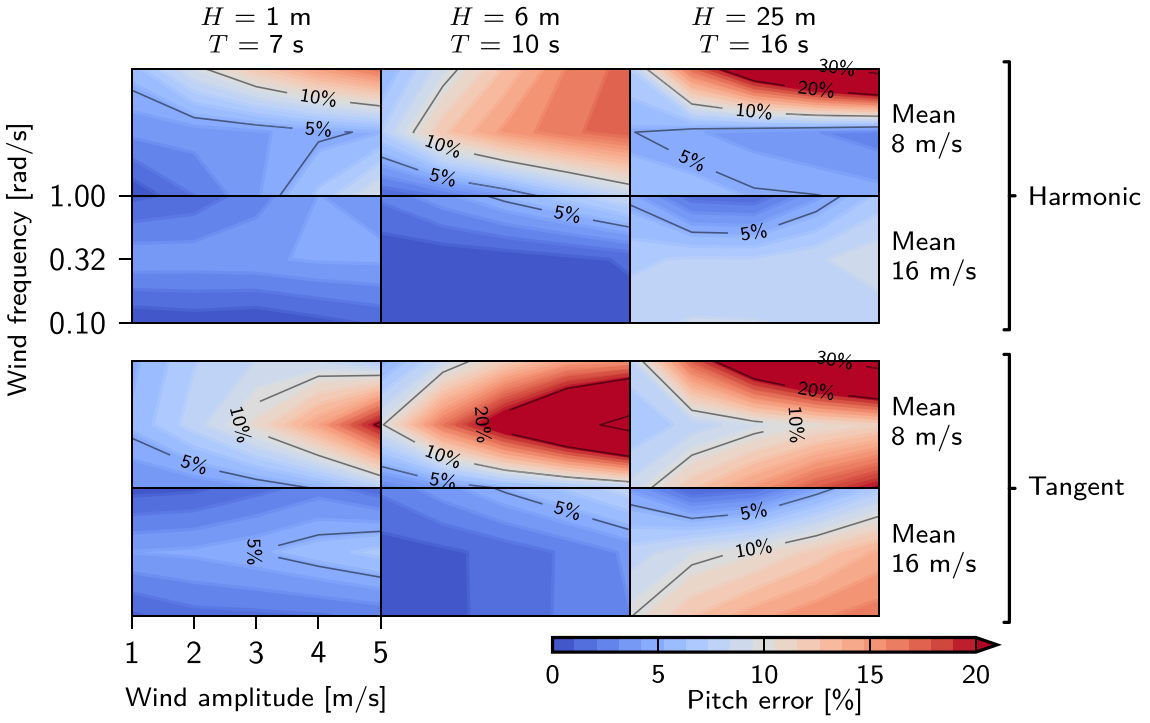

FIGURE 5 Normalised peak–peak error between nonlinear (Bladed) and harmonic solutions in pitch response

nonlinearity was seen in the aerodynamic forces at higher mean wind speeds. The largest errors in the surge response are seen for smaller waves at low wind frequencies, and these will be investigated too in Section 6.2.

The error in the tower deflection response (Figure 6) is mostly acceptable. With 1-m waves, the relative error is greater than 10%, but the response is also small here.

The blade deflection error is shown in Figure 7. The error is acceptable for the smaller waves and smaller variations in wind speed but exceeds 20% for the 25-m waves. The cause of the gradual increase in error with the wind variation amplitude is discussed in Section 6.1, and the larger increase for the biggest waves is discussed in Section 6.2.

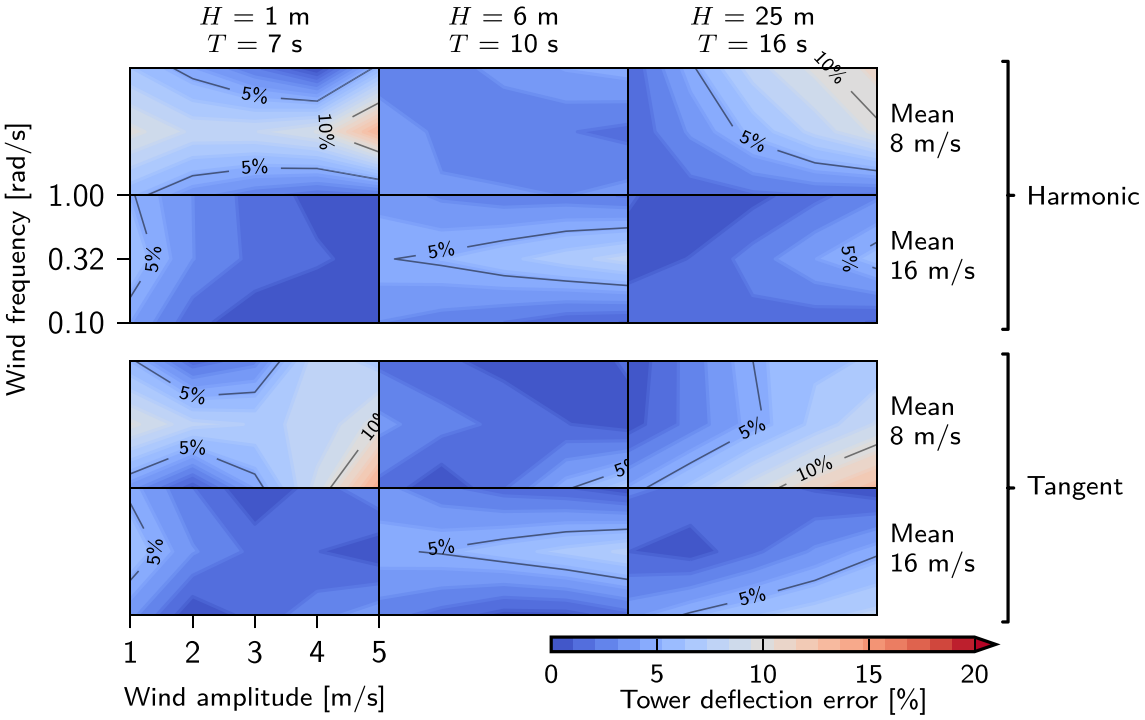

FIGURE 6 Normalised peak–peak error between nonlinear (Bladed) and harmonic solutions in tower deflection response

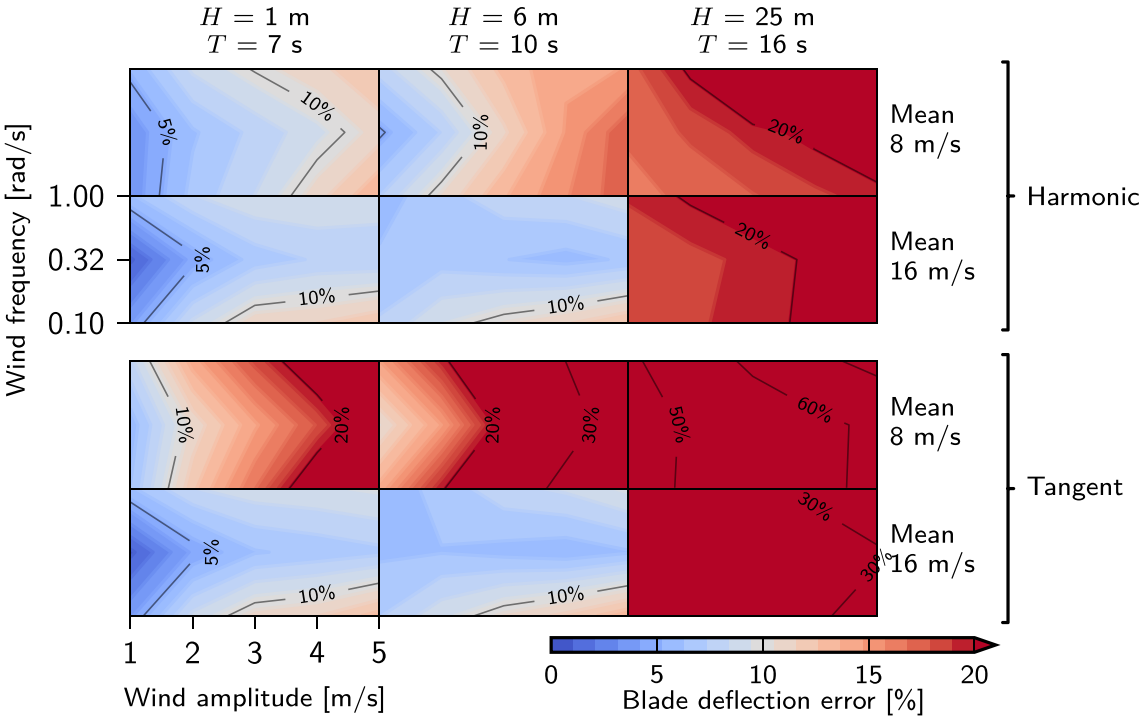

FIGURE 7 Normalised peak–peak error between nonlinear (Bladed) and harmonic solutions in blade deflection response

5.2 | Comparison of tangent and harmonic linearisations

Comparing the two linearisation techniques gives mixed results. Figure 8 plots the ratio of the tangent and harmonic errors for each mean wind speed and sea state.

Most often, the harmonics linearisation gives a lower peak–peak error than the tangent linearisation. The gains are most consistent in the blade deflection, which is consistent with the better performance of the harmonic linearisation seen in Lupton and Langley[35] when dealing with the aerodynamic forces alone. The surge and pitch responses also benefit from the harmonic linearisation, although there are some cases where the tangent linearisation error is smaller. On the other hand, the tower deflection error is generally slightly better with the tangent rather than harmonic linearisation, but the errors are relatively small in these cases. The heave response error is mostly unaffected by the linearisation method; this is because the heave error is due to effects which apply to both methods, as discussed in Section 6.2 below.

5.3 | Comparison of error (with controller active)

Now the control system is reintroduced into the simulations. Figure 9 shows the peak–peak error (Section 4.4) between the harmonic linearisation and the nonlinear Bladed simulations for the conditions which have been run with the control system active. Generally, by adding the control system, the errors have increased by up to 15%. Although the error in the control variables is large, especially the blade pitch angle, this does not carry through into equally large errors in the overall response.

Overall, the change in response due to adding the control system is large compared to the errors, and the linearised system is successful in representing this. This can be seen in Figure 10, which shows the spectrum of the aerodynamic thrust load for the same conditions, with and without the controller active. For the mean wind speed of 8 m s^{-1} (above), the presence of the controller increases the variation in the aerodynamic thrust, while for the mean wind speed of 16 m s^{-1} (below), the controller acts to reduce the variations in thrust. In both cases, the agreement between the linearised and nonlinear results is good compared to the scale of the change due to introducing the controller. The change in aerodynamic thrust carries through to similar changes in the blade deflection and platform surge responses (not shown).

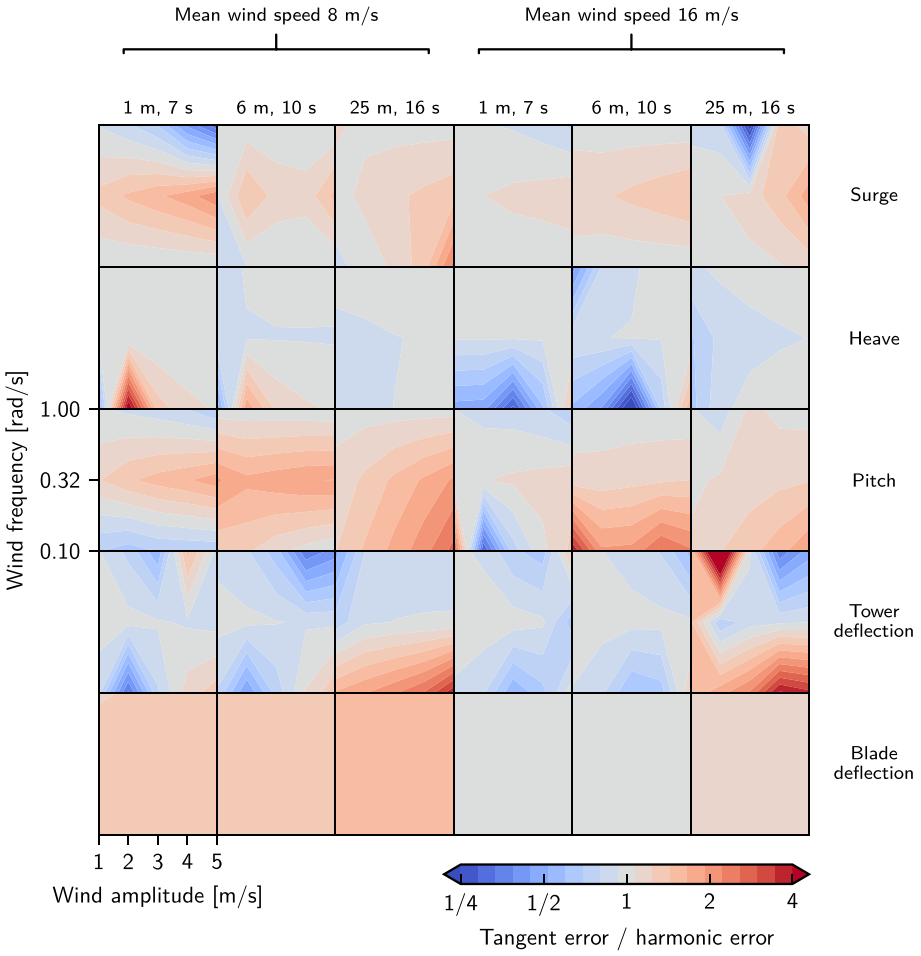

FIGURE 8 Error in tangent linearisation compared to harmonic linearisation. Each column relates to particular mean wind speed and sea state. Each subplot has the same axes as the error plots in Figures 4–7 above

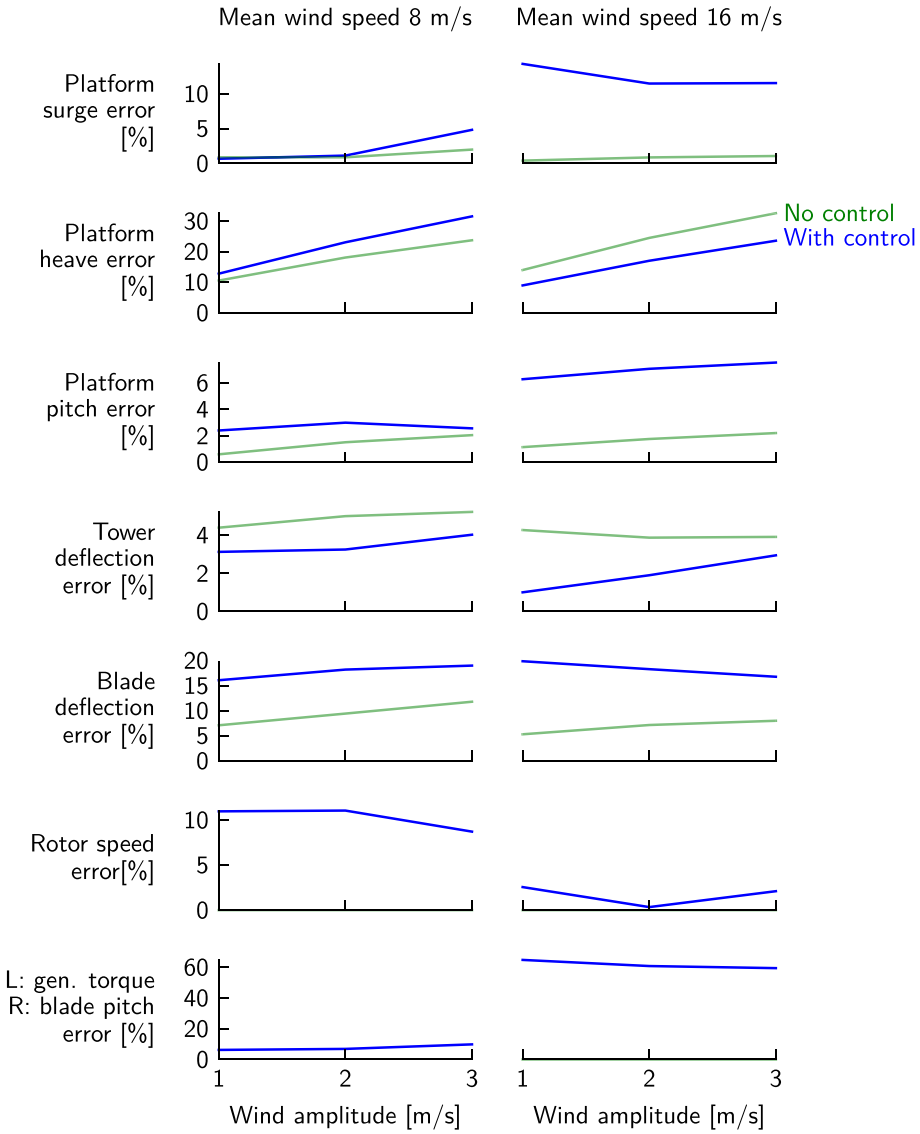

FIGURE 9 Peak–peak error in results including control system, compared to previous results with no control

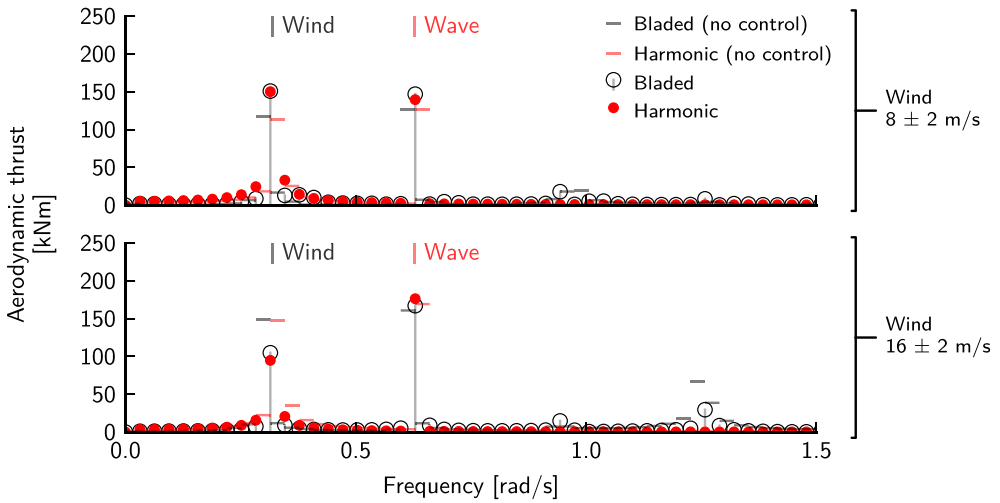

FIGURE 10 Spectrum of aerodynamic thrust with control system, at two mean wind speeds. At 8 m s^{-1}, adding the control system increases the thrust variation, while at 16 m s^{-1}, the variation is reduced. These changes are also seen in the linearised results

TABLE 2 Calculation time relative to Bladed for linearised solutions

		No control		With control
ω (rad s^{-1})	T (s)	Harmonic	Tangent	Harmonic
0.10	7	42%	2.9%	
0.10	10	30%	2.8%	
0.10	13	21%	2.7%	
0.32	7	14%	2.9%	
0.32	10	175%	2.7%	63%
0.32	13	7%	2.7%	
1.00	7	13%	2.8%	
1.00	10	7%	2.7%	
1.00	13	36%	2.7%	

Note. There is little dependence on the mean wind speed, wind variation amplitude and wave height; the mean value over all these variables has been taken. The harmonic solution time with control is normalised against the Bladed solution time with control.

5.4 | Computational time comparison

All calculations were run on an Intel Core i7-2600 3.4 GHz processor. The Bladed simulations of the floating wind turbine without the control system were consistent across all cases, taking 900 to 1,000 s to run. The tangent linearisation calculation was also consistent across all the cases, taking 27 to 29 s to run. The harmonic linearisation, on the other hand, was much more dependent on the wind and wave frequencies involved in the calculation, as shown in Table 2. Calculation times varied between about 70 to 1,750 s.

Part of the difference in calculation speed is due to the linearisation algorithm and part to the speed of the implementation. The linearised results presented here were calculated using Python scripts, whereas Bladed is an optimised commercial code. To estimate how much the implementation speed contributes to the results, a time-domain integration was performed using the same underlying Python code as used for the linearisation. The difference between the run times of this Python code and Bladed represents the differences due to implementation, rather than the difference between the linearised and nonlinear approaches. From this, the present implementation is estimated to be about 40 times slower than Bladed. Using this factor to compensate for the slower implementation of the linearised models, the harmonic solution is estimated to be 20–500 times faster than the time-domain solution. In the same way, the tangent solution is estimated to be 1,200 times faster.

There are two main reasons for the variability of the harmonic linearisation calculations: evaluating the harmonics of the nonlinear functions and solving the nonlinear equations. The harmonics of the nonlinear functions are calculated using a FFT approach described in Section 3.3, but the efficiency of this is dependent on the relative frequencies of the harmonics involved: if the frequencies of the harmonics are close in the frequency domain, the nonlinear function is evaluated over a long sample in the time domain. Solving the nonlinear algebraic equations is achieved using a standard multidimensional root-finding algorithm (a Powell hybrid method[45]). The efficiency of this algorithm determines the number of times the nonlinear functions must be evaluated and therefore directly influences the total calculation time. Little work has been put into improving the efficiency of these algorithms, so it seems likely that improvements could be made.

Adding the control system dynamics into the model increases the duration of both the Bladed simulations and the harmonic linearisation calculation. The harmonic linearisation time has been increased by a factor of 3 and the Bladed simulations times are increased by a factor of 6 on average.

6 | DISCUSSION

The results in Section 5 show substantial variation in the accuracy of the linearised results for different response variables and operating conditions. What causes this inaccuracy? In some cases, it can be seen that the linearised results include the correct harmonics but with inaccurate magnitudes. In other cases, the error is due to the presence of harmonics in the nonlinear response which are entirely missing in the linearised results.

6.1 | Inaccuracies due to linearisation

For example, consider the blade deflection results for 25-m, 16-s waves, wind speed 8 ± 1 m s^{-1} at 0.32 rad s^{-1}. Figure 7 showed quite large errors for these conditions, and Figure 11 shows the time series of the corresponding simulation results. The prediction of the aerodynamic thrust

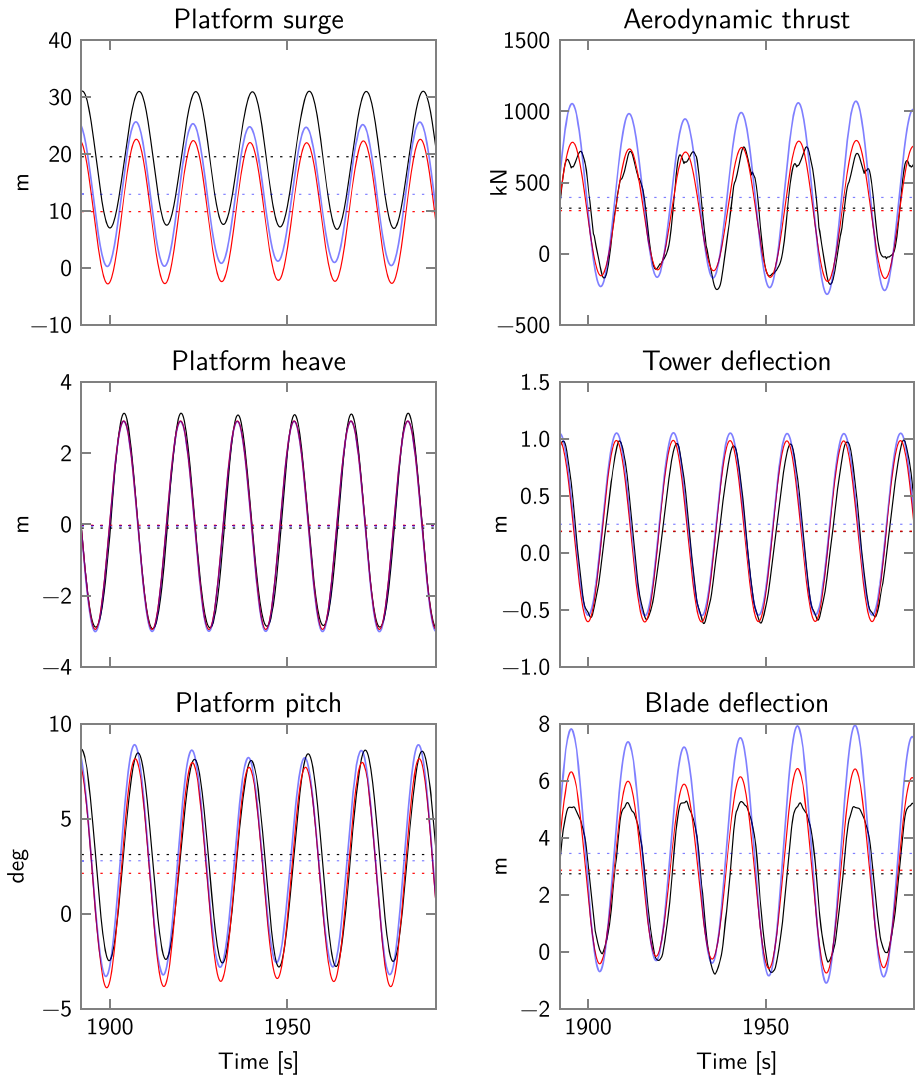

FIGURE 11 Response with 25-m, 16-s waves, wind speed $8 \pm 1\ \mathrm{m\,s^{-1}}$ at $0.32\ \mathrm{rad\,s^{-1}}$. Black: nonlinear (Bladed); red: harmonic; blue: tangent. Dotted lines show the mean value. The difference between the mean values of the nonlinear and linearised results for the platform motion is greater here than in other examples, because of the way the nonlinear wave loading in Bladed has a greater effect in large waves (see Section 4.3)

(top right) is quite good for the harmonic linearisation model and noticeably better than the tangent linearisation results, as previously seen in Lupton and Langley.[35] The blade deflection response (bottom right) is overpredicted, causing the error seen in Figure 7, but the *structure* of the response is largely correct.

6.2 | Inaccuracies due to missing harmonics

Now consider Figure 12, which shows similar conditions to Figure 11 but with a larger amplitude of wind speed variations of $1\ \mathrm{m\,s^{-1}}$. The responses are no longer simple sinusoids, indicating that additional harmonics are present.

This can be seen more clearly in the spectrum, which is shown in Figure 13 for the same cases. For the smaller variations in wind speed, the correct harmonics are included, but the amplitudes do not exactly match. Note that the harmonic linearisation gives much better results than the tangent linearisation in this case, due to the better representation of the nonlinear aerodynamic forces. The error can be traced directly to the aerodynamic thrust, which is also shown in Figure 13. At larger amplitudes, the component of the thrust at the difference frequency $\omega_{\mathrm{wave}} - \omega_{\mathrm{wind}}$ is increased. This component is due to the fact that Bladed is using a spatial wind field, as shown in Figure 2.

Another case with large errors, with a slightly different explanation, was the platform heave response shown in Figure 3. The responses for this case are shown in detail in Figure 14, and it can be seen that the platform heave response has a harmonic component at twice the low-frequency wind variation. The reason for the heave error is the vertical component of the aerodynamic thrust which varies as the platform rotates: the rotor thrust T is assumed to act perpendicular to the rotor plane, so if the platform pitch angle is ϕ, there are horizontal and vertical force contributions of

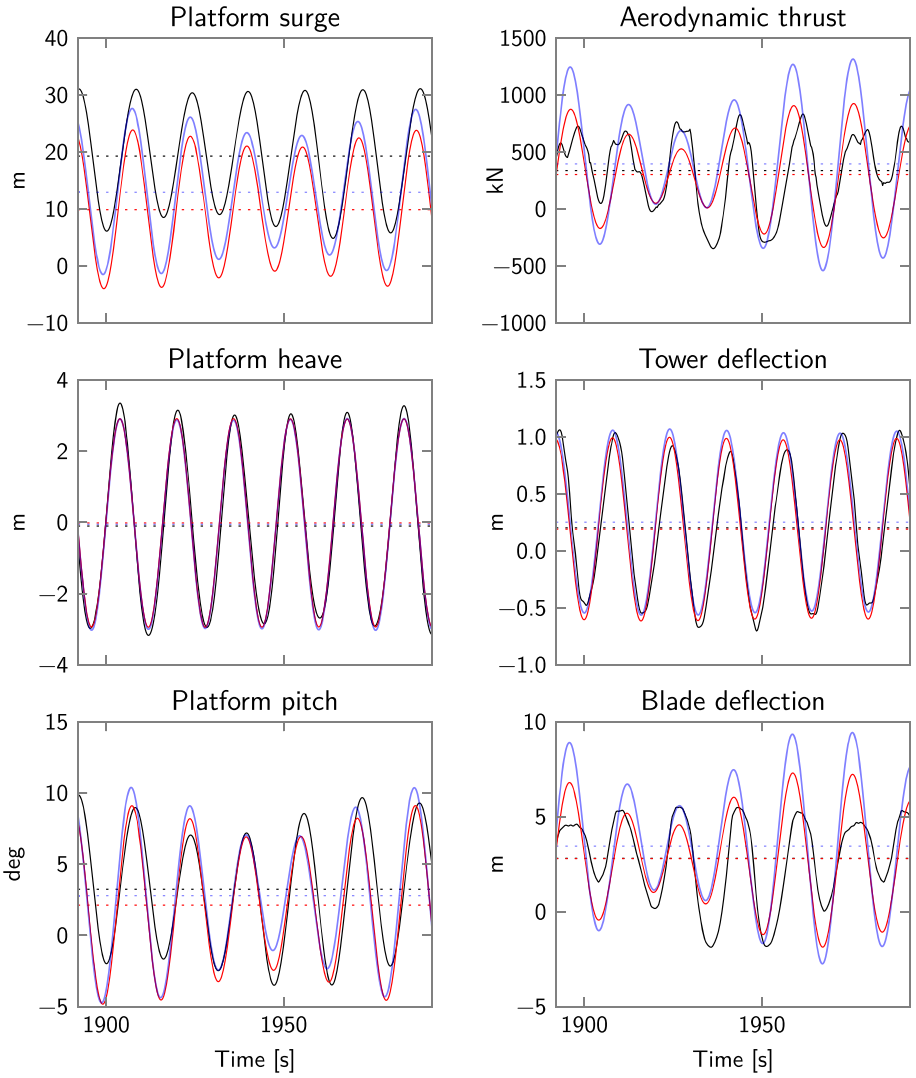

FIGURE 12 Detailed results: same as previous figure but for larger variations in wind speed of $8 \pm 5\ \mathrm{m\,s^{-1}}$

$$F_x = T\cos\phi \text{ and } F_z = -T\sin\phi, \tag{34}$$

respectively. The vertical force therefore has components at the sum and difference of the wind and pitching frequencies. Since the pitching motion in this case is mostly occurring at the wind frequency, the wind-induced heave motion occurs at twice the wind frequency (Figure 15). It is not possible to represent this motion with the two available components of the harmonic solution as implemented here.

In the larger waves (6 and 25 m), the error shown in Figure 3 is reduced because the heave response is caused to a greater extent by the linear wave excitation. As the wind variation increases, the error increases because the nonlinear effect of Bladed's spatial wind field discussed above again becomes important. For example, Figure 16 shows the spectrum of the platform pitch and heave responses with 6-m waves and a wind frequency of $0.32\ \mathrm{rad\,s^{-1}}$. Although it appears that a component at the wind frequency is missing in the linearised results, in fact, the missing harmonic is at $\omega_{\mathrm{wave}} - \omega_{\mathrm{wind}}$; by coincidence, the difference frequency is close to the wind frequency for this case. The large errors in the remaining cases in Figure 3 are likewise caused by missing harmonics in the linearised response.

6.3 | Why does the tangent linearisation sometimes give more accurate results than the harmonic linearisation?

The comparison of the accuracy of the harmonic and tangent linearisation approaches in Section 5.2 showed mixed results, with different methods giving better results in different situations. Given that the harmonic linearisation approach is based on the minimisation of the mean squared error between the nonlinear and linear functions, it may seem strange that in some cases, the tangent linearisation gives a smaller error.

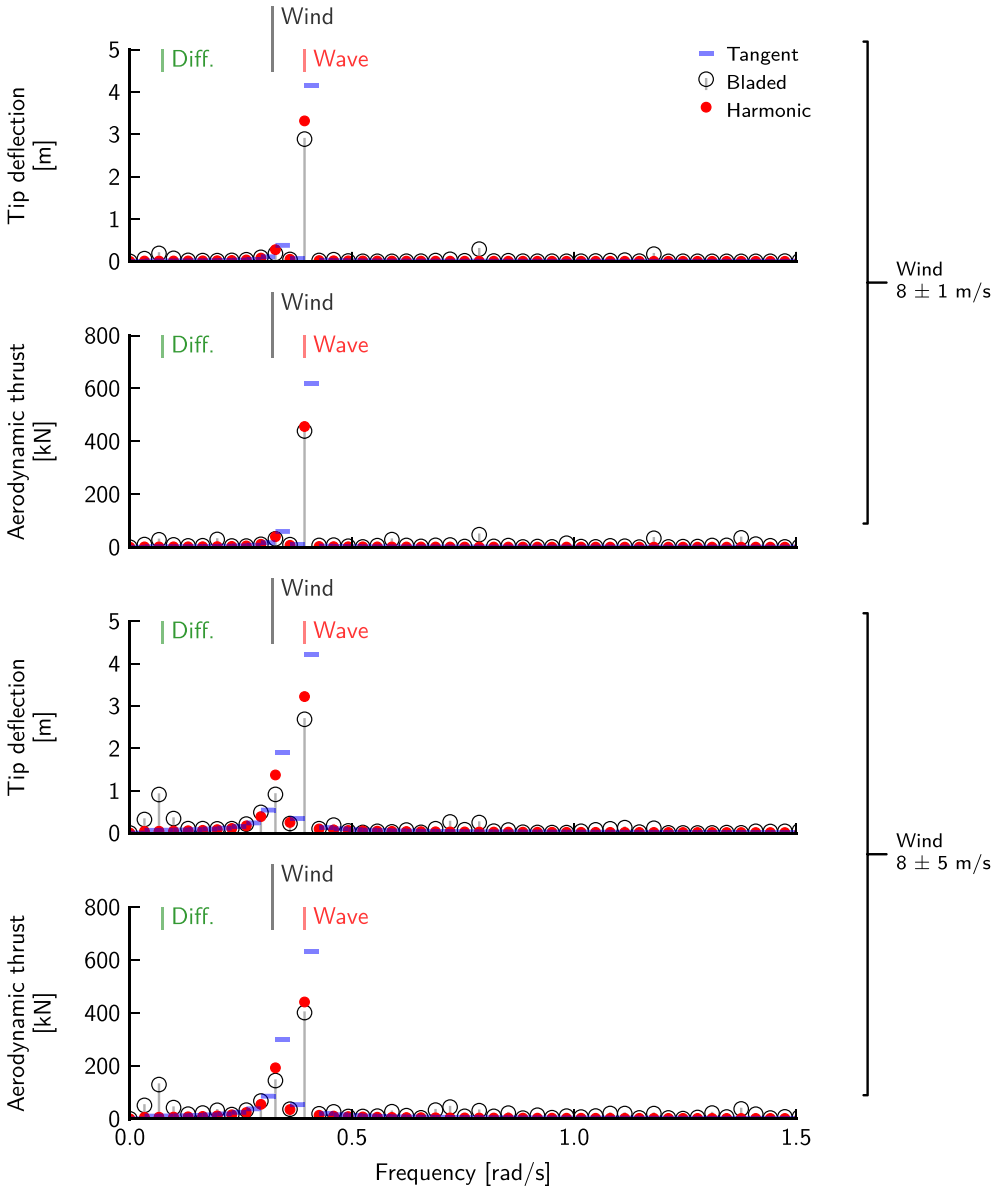

FIGURE 13 Top two plots: spectrum of blade deflection response and aerodynamic thrust with 25-m, 16-s waves, wind speed 8 ± 1 m s^{-1} at 0.32 rad s^{-1}. Bottom two plots: as above but for 8 ± 5 m s^{-1} wind. For small variations in wind speed (top), the error is due to the amplitude of the linearised response. When the wind speed variations are large (bottom), there is also some nonlinear response at $\omega_{\text{wave}} - \omega_{\text{wind}}$ (labelled 'Diff.'). The blade deflection is closely linked to the thrust

This is because the results in this chapter (including Figure 8) are based on the peak–peak error, as defined in Equation (33), and minimising the mean squared error does not necessarily minimise the peak–peak error. Figure 17 presents a contrived example which demonstrates this. However, when the tangent linearisation gives a lower peak–peak error, it is only through good luck, and the harmonic linearisation should be more robust in the face of a variable level of nonlinearity.

6.4 | Capturing additional harmonics in the calculated nonlinear forces

Section 6.2 has shown that many of the errors in the linearised model are due to missing harmonics that are present in the full nonlinear results of the model. This raises the question of whether these additional harmonics could be captured within an extended linearised model.

In principle, Equation (17) could be extended to include a response at an additional frequency (such as double the wind frequency, $2\omega_1$, as seen in Figure 15). While this could improve the accuracy of the predicted response, it would come at a cost as it would introduce additional harmonic balance equations into Equation (27) (specifically, two real equations or one complex equation per additional harmonic), which would affect the solution time and convergence of the solution.

However, there is some information on additional harmonics already available without additional calculations. The nonlinear function $\boldsymbol{f}(t)$ from Equation (18) is calculated numerically based on the harmonic input $\boldsymbol{x}(t)$. In Equation (21), only its first harmonics at ω_1 and ω_2 are kept, but in fact, additional harmonics in the response could be extracted which might be expected to improve the accuracy of the result. This represents a

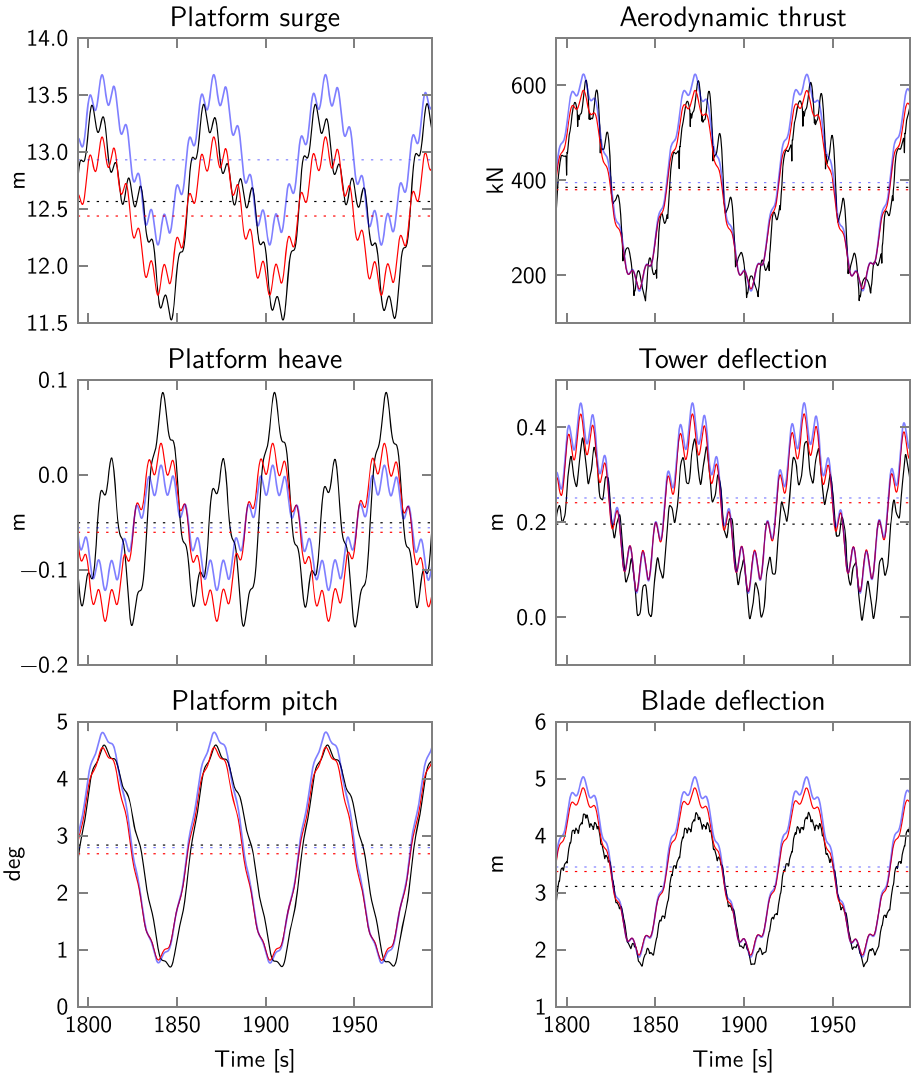

FIGURE 14 Response with 1-m, 7-s waves, wind speed $8 \pm 3\ \mathrm{m\,s^{-1}}$ at 0.1 rad $\mathrm{s^{-1}}$. Black: nonlinear (Bladed); red: harmonic; blue: tangent. The low-frequency variation is at ω_{wind} and the high-frequency oscillation is at ω_{wave}. The heave motion occurs at $2\omega_{\mathrm{wind}}$, which is not captured by the linearised models (see text and Figure 15). The surge motion occurs mostly at ω_{wind}, but the linearised results are also missing a component at $2\omega_{\mathrm{wind}}$

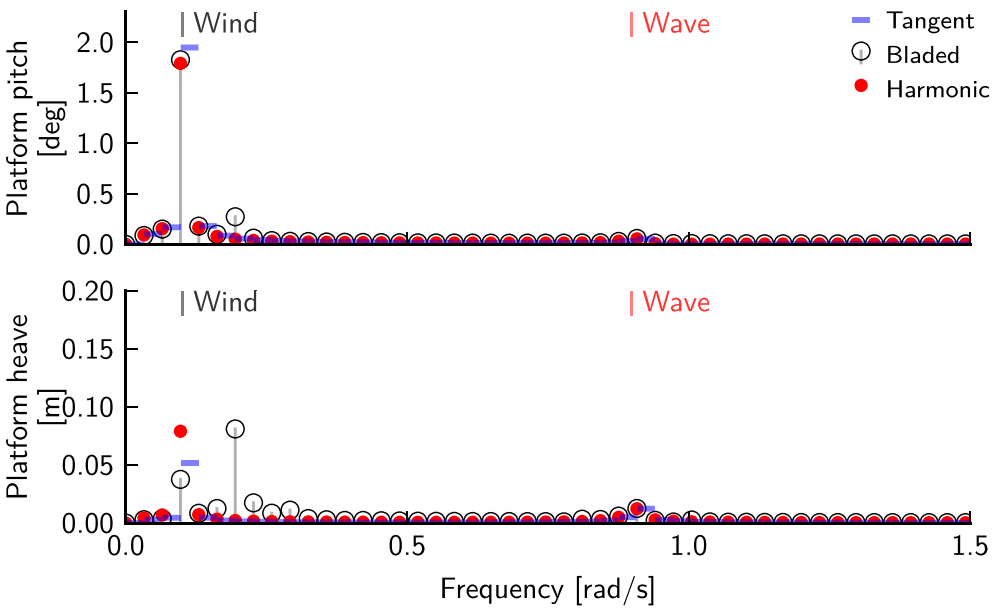

FIGURE 15 Spectrum of heave response with 1-m, 7-s waves, wind speed $8 \pm 3\ \mathrm{m\,s^{-1}}$ at 0.1 rad $\mathrm{s^{-1}}$. The platform pitching motion at the wind frequency combines with the aerodynamic thrust to produce a heave motion at twice the wind frequency, which is not included in the linearised models

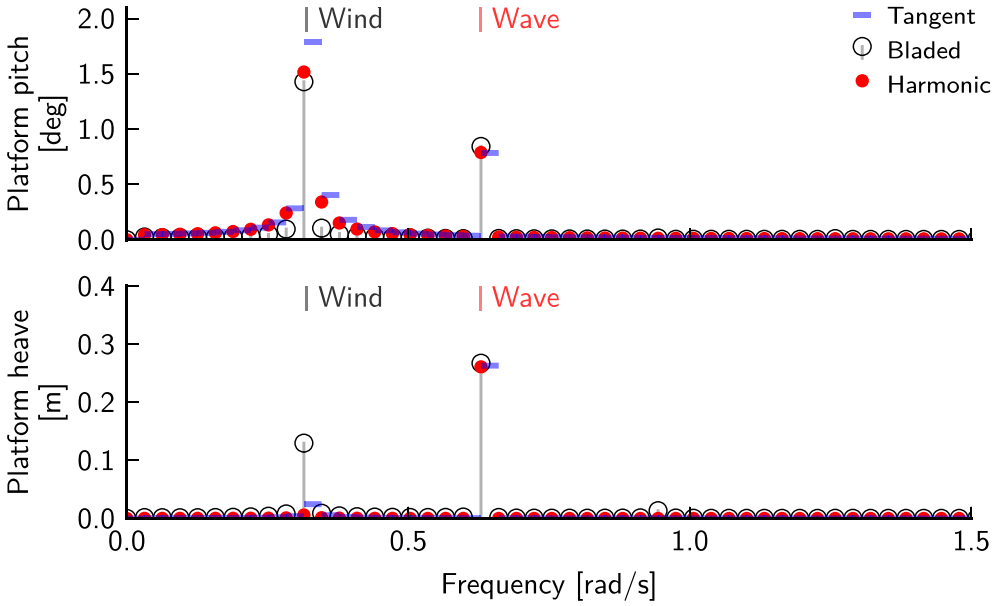

FIGURE 16 Spectrum of heave response with 6-m, 10-s waves, wind speed $8 \pm 5\ \mathrm{m\,s^{-1}}$ at $0.32\ \mathrm{rad\,s^{-1}}$. The missing harmonic is at $\omega_{\mathrm{wave}} - \omega_{\mathrm{wind}}$; by coincidence, the difference is close to the wind frequency

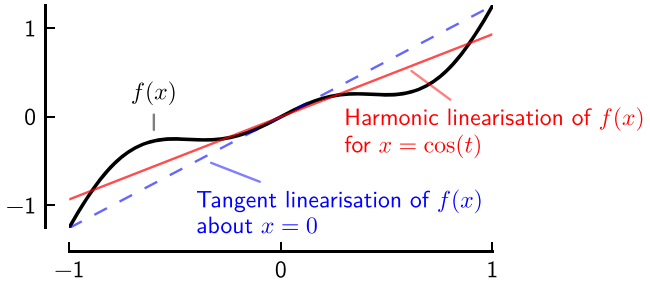

FIGURE 17 A contrived example to show that while the harmonic linearisation minimises the mean squared error, it does not necessarily minimise the peak–peak error

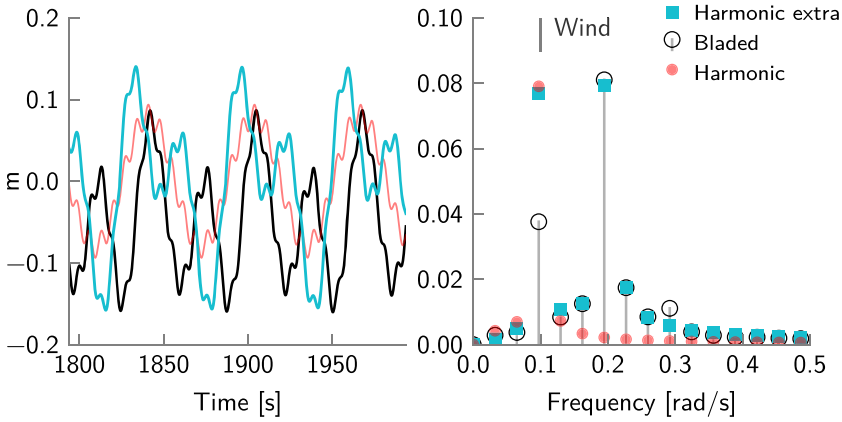

FIGURE 18 Platform heave response including an additional harmonic as a post-processing step. The wind and wave conditions and the Bladed (black) and harmonic (red) results are the same as in Figures 14 and 15. The 'harmonic extra' response includes the $2\omega_1$ harmonic of the calculated nonlinear forces

half-step towards the full extended harmonic balance method described in the paragraph above: additional harmonics in the response could be reported as a post-processing step, but they would not be taken into account as part of the iterative solution of Equation (27).

Figure 18 shows an example of this, corresponding to the case previously seen in Figures 14 and 15, where the error in the linearised response was attributed to a missing harmonic at $2\omega_1$. Based on the solution found by harmonic linearisation at the two base frequencies ω_1 and ω_2, the spectrum shows that the response at $2\omega_1$ is fairly well estimated by this approach, in this case. However, the magnitude of the first harmonic at ω_1 is overestimated, leading to the overall response amplitude being too large. This makes sense intuitively, as in the initial harmonic linearisation, the magnitude of the response at ω_1 is increased to approximate the missing response at $2\omega_1$. If the $2\omega_1$ harmonic were to be included within the iterative solution of Equation (27), subsequent iterations would be expected to reduce the magnitude of the harmonic at ω_1 such that the overall response better matched the nonlinear response.

This example shows that while this type of post-processing could potentially lead to improved accuracy by including missing harmonics, if there is significant spectral content at these higher harmonics present, predicted magnitudes are unlikely to be accurate. On the other hand, if the predicted magnitude of the higher harmonics is small, then that could be a useful indication that that linearised model is performing adequately.

7 | CONCLUSIONS

The main aim of this paper was to test the harmonic linearisation of the aerodynamic loads and control system behaviour in the context of a complete model of a floating wind turbine—to quantify its performance over a range of operating conditions but also, in cases where the accuracy is unsatisfactory, to give some insight into the causes.

Overall, these results show that it is possible to create a frequency-domain model of a floating wind turbine with a high level of detail: a flexible structure, aeroelastic rotor loads and the effect of the control system. Although the results are approximate, it seems that reasonable accuracy is achievable. The influence of the control system is effectively captured (the change in behaviour when enabling it is large compared to the linearisation errors), although there are unaddressed issues remaining with accuracy around rated wind speed.[35] Of course, the results presented here form a case study of just one design of floating wind turbine, and different levels of accuracy might be achieved in designs with very different response characteristics.

Some inaccuracy is due to inaccurate linearisation of magnitudes of nonlinear aerodynamic forces (the issue addressed by previous work on the aerodynamic loads in isolation[35]), but a bigger issue proved to be the presence of additional harmonics caused by nonlinear interactions between loading at different frequencies. These can have a dominant effect on the peak–peak error of many response variables. In principle, the model could be extended to include these interaction frequencies, at the expense of an increased number of system equations (like Equation 27) to be solved.

In many cases, the computational cost of the harmonic linearisation is of the order of 10 times slower than the tangent linearisation and 100 times faster than the time-domain solution. In some cases where the wind and wave loading frequencies interact poorly, the harmonic solution can slow down, but it may be possible to improve the implementation to mitigate this.

Finally, this work has focused on modelling the response to harmonic inputs. This is directly useful in some situations, but in others, the response to stochastic inputs (turbulent wind and random seas) is more relevant. Further work could build on the understanding of the harmonic case presented here to generalise from harmonic linearisation to stochastic linearisation.

ACKNOWLEDGEMENT

This work was funded by an EPSRC doctoral training award (ref. 1089390) and supported by GL Garrad Hassan. We would like to thank the three anonymous reviewers for their helpful comments.

PEER REVIEW

The peer review history for this article is available at https://publons.com/publon/10.1002/we.2605.

ORCID

Richard C. Lupton https://orcid.org/0000-0001-8622-3085

REFERENCES

1. Nielsen FG, Hanson TD, Skaare B. Integrated Dynamic Analysis of Floating Offshore Wind Turbines. In: Proceedings of the 25th International Conference on Offshore Mechanics and Arctic Engineering. Volume 1: Offshore Technology; Offshore Wind Energy; Ocean Research Technology; LNG Specialty Symposium ASME; 2006; Hamburg, Germany:671-679. https://doi.org/10.1115/OMAE2006-92291
2. Roddier D, Cermelli C, Aubault A, Weinstein A. WindFloat: a floating foundation for offshore wind turbines. *J Renew Sustain Energy*. 2010;2(3):33104. https://doi.org/10.1063/1.3435339
3. Fukushima Offshore Wind Consortium. https://www.fukushima-forward.jp/english/index.html
4. Matha D, Sandner F, Molins C, Campos A, Cheng PW. Efficient preliminary floating offshore wind turbine design and testing methodologies and application to a concrete spar design. *Philos. Trans. R. Soc. A Math. Phys. Eng. Sci.* 2015;373(2035):20140350. https://doi.org/10.1098/rsta.2014.0350
5. The Carbon Trust. Floating Offshore Wind: Market & Technology Review. *Technical report*; 2015. https://www.carbontrust.com/media/670664/floating-offshore-wind-market-technology-review.pdf
6. Wind Europe. Offshore wind in Europe: key trends and statistics 2017. *Technical report*; 2018. https://windeurope.org/wp-content/uploads/files/about-wind/statistics/WindEurope-Annual-Offshore-Statistics-2017.pdf
7. Muskulus M, Schafhirt S. Design optimization of wind turbine support structures—a review. *J Ocean Wind Energy*. 2014;1(1):11 en.
8. Jonkman J, Buhl MLJ. FAST Users' Guide. *Technical report*, NREL; 2005. https://www.nrel.gov/docs/fy06osti/38230.pdf
9. Garrad Hassan. Bladed Theory Manual. *Technical report*. version 4.1; 2011.
10. Pegalajar-Jurado A, Borg M, Bredmose H. An efficient frequency-domain model for quick load analysis of floating offshore wind turbines. *Wind Energy Sci*. 2018;3(2):693-712 English. https://doi.org/10.5194/wes-3-693-2018
11. Hall M, Buckham B, Crawford C. Evolving offshore wind. In: A genetic algorithm-based support structure optimization framework for floating wind turbines. Bergen, Norway, IEEE; 2013:1-10. https://doi.org/10.1109/OCEANS-Bergen.2013.6608173
12. Matha D, Sandner F, Schlipf D. Efficient critical design load case identification for floating offshore wind turbines with a reduced nonlinear model. *J Phys: Conf Ser*. 2014;555:12069. https://doi.org/10.1088/1742-6596/555/1/012069
13. Jonkman JM. Dynamics Modeling and Loads Analysis of an Offshore Floating Wind Turbine. *Technical Report*. NREL/TP-500-41958, 921803; 2007.

14. Bae YH, Kim MH, Im SW, Chang IH. Aero-elastic-control-floater-mooring coupled dynamic analysis of floating offshore wind turbines. In: Proceedings of the 21st International Society of Offshore and Polar Engineers (ISOPE); 2011:429-435.
15. Karimirad M, Moan T. A simplified method for coupled analysis of floating offshore wind turbines. *Marine Struct*. 2012;27(1):45-63. https://doi.org/10.1016/j.marstruc.2012.03.003
16. Lupton RC, Langley RS. Complex but negligible: non-linearity of the inertial coupling between the platform and blades of floating wind turbines. *Renew Energy*. 2019;134:710-726. https://doi.org/10.1016/j.renene.2018.11.036
17. Fujiwara H, Tsubogo T, Nihei Y. Gyro effect of rotating blades on the floating wind turbine platform in waves. *Proc Int Offshore Polar Eng Conf*. 2011;8:399-406.
18. Sandner F, Schlipf D, Matha D, Seifried R, Cheng PW. Reduced nonlinear model of a spar-mounted floating wind turbine. In: Proceedings of the 11th German Wind Energy Conference DEWEK 2012; 2012; Bremen, Germany. https://doi.org/10.18419/opus-4528
19. Sandner F, Schlipf D, Matha D, Cheng PW. Integrated optimization of floating wind turbine systems. In: International Conference on Offshore Mechanics and Arctic Engineering American Society of Mechanical Engineers; 2014:V09BT09A030. https://doi.org/10.1115/OMAE2014-24244
20. Halfpenny A. Dynamic Analysis of Both On and Offshore Wind Turbines in the Frequency Domain. *Ph.D. Thesis*. London: University College; 1998.
21. Merz KO, Muskulus M, Moe G. A simple frequency-domain method for stress analysis of stall-regulated wind turbines: frequency-domain analysis of stall-regulated turbines. *Wind Energy*. 2012;15(5):773-798. https://doi.org/10.1002/we.504
22. van Engelen TG. Frequency Domain Analysis of Offshore Wind Turbines. *Technical report*, ECN; 2004.
23. van der Male P, van Dalen KN, Metrikine AV. The effect of the nonlinear velocity and history dependencies of the aerodynamic force on the dynamic response of a rotating wind turbine blade. *J Sound Vib*. 2016;383:191-209. https://doi.org/10.1016/j.jsv.2016.07.031
24. Durá FE, Gimenez FM, Corretge JS. Fast estimation of the damage equivalent load in blade geometry multidisciplinary optimization. *J Solar Energy Eng*. 2017;139(4):41008. https://doi.org/10.1115/1.4036636
25. Karimi M, Hall M, Buckham B, Crawford C. A multi-objective design optimization approach for floating offshore wind turbine support structures. *J Ocean Eng Marine Energy*. 2017;3(1):69-87. https://doi.org/10.1007/s40722-016-0072-4
26. Kluger JM, Sapsis TP, Slocum AH. A reduced-order, statistical linearization approach for estimating nonlinear floating wind turbine response statistics. In: The 26th International Ocean and Polar Engineering Conference International Society of Offshore and Polar Engineers; 2016:545-552.
27. Fontanella A, Bayati I, Belloli M. Linear coupled model for floating wind turbine control. *Wind Eng*. 2018;42(2):115-127. https://doi.org/10.1177/0309524X18756970
28. Jonkman JM, Jonkman BJ. FAST modularization framework for wind turbine simulation: full-system linearization. *J Phys: Conf Ser*. 2016;753:82010. https://doi.org/10.1088/1742-6596/753/8/082010
29. Lee KH. Responses of Floating Wind Turbines to Wind and Wave Excitation. *Ph.D. Thesis*: MIT / MIT; 2005.
30. Elishakoff I, Crandall SH. Sixty years of stochastic linearization technique. *Meccanica*. 2017;52(1-2):299-305. https://doi.org/10.1007/s11012-016-0399-x
31. Langley RS. The linearisation of three dimensional drag force in random seas with current. *Appl Ocean Res*. 1984;6(3):126-131.
32. Savenije FJ, Peeringa JM. Aero-elastic simulation of offshore wind turbines in the frequency domain. *Technical report*; 2009.
33. Lupton RC. Frequency-Domain Modelling of Floating Wind Turbines. *Ph.D. Thesis*: University of Cambridge; 2015. https://doi.org/10.17863/CAM.14119
34. Lemmer F, Yu W, Cheng PW. Iterative frequency-domain response of floating offshore wind turbines with parametric drag. *Journal of Marine Science and Engineering*. 2018;6(4):118. https://doi.org/10.3390/jmse6040118
35. Lupton RC, Langley RS. Improved linearised models of wind turbine aerodynamics and control system dynamics using harmonic linearisation. *Renew Energy*. 2019;135:148-162. https://doi.org/10.1016/j.renene.2018.11.067
36. Borgman LE. Random hydrodynamic forces on objects. *Annal Math Stat*. 1967;38(1):37-51. https://doi.org/10.1214/aoms/1177699057
37. Jonkman J. Definition of the Floating System for Phase IV of OC3. *Technical Report*. NREL/TP-500-47535, Golden, USA, National Renewable Energy Laboratory / National Renewable Energy Laboratory; 2010.
38. Cummins WE. The impulse response function and ship motions. *Symp Ship Theory*. 1962;9:101-109.
39. Lupton RC. Mbwind v1.0; 2018. http://doi.org/10.5281/zenodo.1221056
40. Hansen MH. Aeroelastic instability problems for wind turbines. *Wind Energy*. 2007;10(6):551-577. https://doi.org/10.1002/we.242
41. Faltinsen OM. *Sea Loads on Ships and Offshore Structures*. Cambridge: Cambridge University Press; 1993.
42. Lupton R. Ricklupton/bemused: V0.2.0. Zenodo; 2019. http://doi.org/10.5281/zenodo.3356689
43. Jonkman J, Butterfield S, Musial W, Scott G. Definition of a 5-MW Reference Wind Turbine for Offshore System Development. *Technical Report*. NREL/TP-500-38060, National Renewable Energy Laboratory; 2009. https://www.nrel.gov/docs/fy09osti/38060.pdf
44. Langley RS. Harmonic linearisation of geometrically non-linear finite element models. *Comput Struct*. 1988;28(2):165-172. https://doi.org/10.1016/0045-7949(88)90036-3
45. Jones E, Oliphant T, Peterson P, others. SciPy: Open source scientific tools for Python. https://www.scipy.org/; 2001.
46. IEC. *IEC 61400-1:2005: Wind turbines - Part 1: Design requirements*. Third edition. Geneva, Switzerland: IEC; 2005. https://webstore.iec.ch/publication/5427
47. Schløer S, Garcia Castillo L, Fejerskov M, Stroescu E, Bredmose H. A model for quick load analysis for monopile-type offshore wind turbine substructures. *Wind Energy Sci*. 2018;3(1):57-73. https://doi.org/10.5194/wes-3-57-2018

How to cite this article: Lupton RC, Langley RS. Harmonic linearisation of aerodynamic loads in a frequency-domain model of a floating wind turbine. *Wind Energy*. 2021;24:833–856. https://doi.org/10.1002/we.2605